OPEN ACCESS



The La Silla Schmidt Southern Survey

```
Adam A. Miller<sup>1,2,3</sup>, Natasha S. Abrams<sup>4</sup>, Greg Aldering<sup>5</sup>, Shreya Anand<sup>4,6,48</sup>, Charlotte R. Angus<sup>7</sup>, Iair Arcavi<sup>8</sup>, Charles Baltay<sup>9</sup>, Franz E. Bauer<sup>10</sup>, Daniel Brethauer<sup>4</sup>, Joshua S. Bloom<sup>4,5</sup>, Hemanth Bommireddy<sup>11</sup>, Márcio Catelan<sup>12,13,14</sup>, Ryan Chornock<sup>4</sup>, Peter Clark<sup>15</sup>, Thomas E. Collett<sup>16</sup>, Georgios Dimitriadis<sup>17</sup>, Sara Faris<sup>8</sup>, Francisco Förster<sup>13,18,19</sup>, Anna Franckowiak<sup>20</sup>, Christopher Frohmaier<sup>15</sup>, Lluís Galbany<sup>21,22</sup>, Renato B. Galleguillos<sup>13,23</sup>, Ariel Goobar<sup>24</sup>, Or Graur<sup>16,25</sup>, Claudia P. Gutiérrez<sup>21,22</sup>, Saarah Hall<sup>1,2</sup>, Erica Hammerstein<sup>4</sup>, Kenneth R. Herner<sup>26</sup>, Isobel M. Hook<sup>17</sup>, Macy J. Huston<sup>4</sup>, Joel Johansson<sup>24</sup>,
             Charles D. Kilpatrick<sup>2</sup>, Alex G. Kim<sup>5</sup>, Robert A. Knop<sup>5</sup>, Marek P. Kowalski<sup>27,28</sup>, Lindsey A. Kwok<sup>2</sup>,
Charles D. Kilpatrick<sup>2</sup>, Alex G. Kim<sup>3</sup>, Robert A. Knop<sup>3</sup>, Marek P. Kowalski<sup>2</sup>, Undsey A. Kwok<sup>2</sup>, Natalie LeBaron<sup>4</sup>, Kenneth W. Lin<sup>4,5</sup>, Chang Liu<sup>1,2</sup>, Jessica R. Lu<sup>4</sup>, Wenbin Lu<sup>4,29</sup>, Ragnhild Lunnan<sup>30</sup>, Kate Maguire<sup>31</sup>, Lydia Makrygianni<sup>17</sup>, Raffaella Margutti<sup>4,32</sup>, Dan Maoz<sup>8</sup>, Patrik Milán Veres<sup>20</sup>, Thomas Moore<sup>7</sup>, A. J. Nayana<sup>4</sup>, Matt Nicholl<sup>7</sup>, Jakob Nordin<sup>28</sup>, S. R. Oates<sup>17</sup>, Giuliano Pignata<sup>10,13</sup>, Abigail Polin<sup>33</sup>, Dovi Poznanski<sup>6,8,34,35</sup>, Jose L. Prieto<sup>13,36</sup>, David L. Rabinowitz<sup>37</sup>, Nabeel Rehemtulla<sup>1,2,3</sup>, Mickael Rigault<sup>38</sup>, Dan Ryczanowski<sup>16,39</sup>, Nikhil Sarin<sup>24,40</sup>, Steve Schulze<sup>2</sup>, Ved G. Shah<sup>1,2,3</sup>, Xinyue Sheng<sup>7</sup>, Samuel P. R. Shilling<sup>17</sup>, Brooke D. Simmons<sup>17</sup>, Avinash Singh<sup>30,41</sup>, Graham P. Smith<sup>39,42</sup>, Mathew Smith<sup>17</sup>, Jesper Sollerman<sup>30</sup>, Maayane T. Soumagnac<sup>5,43</sup>, Christopher W. Stubbs<sup>44,45</sup>, Mark Sullivan<sup>15</sup>, Aswin Suresh<sup>1,2</sup>, Benny Trakhtenbrot<sup>8</sup>,
                Charlotte Ward<sup>46</sup>, Eli Wiston<sup>4</sup>, Helen Xiong<sup>9</sup>, Yuhan Yao<sup>4,47</sup>, and Peter E. Nugent<sup>4,5</sup>
     <sup>2</sup> Center for Interdisciplinary Exploration and Research in Astrophysics (CIERA), Northwestern University, 1800 Sherman Ave, Evanston, IL 60201, USA
                                                     NSF-Simons AI Institute for the Sky (SkAI), 172 E. Chestnut St., Chicago, IL 60611, USA
                                                         Department of Astronomy, University of California, Berkeley, CA 94720-3411, USA
                                          <sup>5</sup> Lawrence Berkeley National Laboratory, 1 Cyclotron Road, MS 50B-4206, Berkeley, CA 94720, USA
                           <sup>6</sup> Kavli Institute for Particle Astrophysics and Cosmology, Stanford University, 452 Lomita Mall, Stanford, CA 94305, USA
                                 Astrophysics Research Centre, School of Mathematics and Physics, Queens University Belfast, Belfast BT7 1NN, UK
                                                             School of Physics and Astronomy, Tel Aviv University, Tel Aviv 69978, Israel
                                             <sup>9</sup> Department of Astronomy, Yale University, P. O. Box 208101, New Haven, CT 06520-8101, USA
                                                          <sup>10</sup> Instituto de Alta Investigación, Universidad de Tarapacá, Casilla 7D, Arica, Chile
                                     <sup>11</sup> Department of Astronomy, Universidad de Chile, Camino el Observatorio 1515, Las Condes, Santiago, Chile
                       <sup>12</sup> Instituto de Astrofísica, Pontificia Universidad Católica de Chile, Av. Vicuña Mackenna 4860, 7820436 Macul, Santiago, Chile Millennium Institute of Astrophysics (MAS), Nuncio Monseñor Sótero Sanz 100, Providencia, Santiago, Chile
                    <sup>14</sup> Centro de Astro-Ingeniería, Pontificia Universidad Católica de Chile, Av. Vicuña Mackenna 4860, 7820436 Macul, Santiago, Chile
                                                    School of Physics and Astronomy, University of Southampton, Southampton, SO17 1BJ, UK
                                    <sup>16</sup> Institute of Cosmology and Gravitation, University of Portsmouth, Burnaby Road, Portsmouth, PO1 3FX, UK
                                                                    Department of Physics, Lancaster University, Lancaster LA1 4YB, UK
                          <sup>18</sup> Data and Artificial Intelligence Initiative (IDIA), Faculty of Physical and Mathematical Sciences, University of Chile, Chile
                                          Center for Mathematical Modeling (CMM), Universidad de Chile, Beauchef 851, Santiago 8320000, Chile
          <sup>20</sup> Ruhr University Bochum, Faculty of Physics and Astronomy, Astronomical Institute (AIRUB), Universitätsstraße 150, 44801 Bochum, Germany
                                      Institute of Space Sciences (ICE-CSIC), Campus UAB, Carrer de Can Magrans, s/n, E-08193 Barcelona, Spain
                                                       Institut d'Estudis Espacials de Catalunya (IEEC), 08860 Castelldefels (Barcelona), Spain
                                          <sup>23</sup> Faculty of Engineering, Finis Terrae University, 1509 Pedro de Valdivia Ave, Providencia, RM, Chile
                                                Oskar Klein Centre, Department of Physics, Stockholm University, SE-10691 Stockholm, Sweden
              Department of Astrophysics, American Museum of Natural History, Central Park West and 79th Street, New York, NY 10024-5192, USA
                                                                         Fermi National Accelerator Laboratory, Batavia, IL 60510, USA
                                                       <sup>27</sup> Deutsches Elektronen Synchrotron DESY, Platanenallee 6, 15738 Zeuthen, Germany
                                                              <sup>28</sup> Institut für Physik, Humboldt-Universität zu Berlin, 12489 Berlin, Germany <sup>29</sup> Theoretical Astrophysics Center, UC Berkeley, Berkeley, CA 94720, USA
                      Oskar Klein Centre, Department of Astronomy, Stockholm University, Albanova University Center, 106 91 Stockholm, Sweden

School of Physics, Trinity College Dublin, College Green, Dublin 2, Ireland
                                       <sup>32</sup> Department of Physics, University of California, 366 Physics North MC 7300, Berkeley, CA 94720, USA
                              <sup>33</sup> Purdue University, Department of Physics and Astronomy, 525 Northwestern Ave, West Lafayette, IN 4790720, USA
                                                   Cahill Center for Astrophysics, California Institute of Technology, Pasadena, CA 91125, USA
                                                Department of Physics, Stanford University, 382 Via Pueblo Mall, Stanford, CA 94305, USA
         <sup>36</sup> Instituto de Estudios Astrofísicos, Facultad de Ingeniería y Ciencias, Universidad Diego Portales, Avenida Ejercito Libertador 441, Santiago, Chile
                                                   Department of Physics, Yale University, P.O. Box 208120, New Haven, CT 06520-8101, USA
                                       <sup>38</sup> Universite Claude Bernard Lyon 1, CNRS, IP2I Lyon/IN2P3, UMR 5822, F-69622, Villeurbanne, France
                                                      School of Physics and Astronomy, University of Birmingham, Birmingham, B15 2TT, UK
                     <sup>40</sup> Nordita, Stockholm University and KTH Royal Institute of Technology, Hannes Alfvéns v ag 12, SE-106 91 Stockholm, Sweden
                   41 Hiroshima Astrophysical Science Centre, Hiroshima University, 1-3-1 Kagamiyama, Higashi-Hiroshima, Hiroshima 739-8526, Japan
                                                Department of Astrophysics, University of Vienna, Türkenschanzstrasse 17, 1180 Vienna, Austria

43 Department of Physics, Bar-Ilan University, Ramat-Gan 52900, Israel
                                                    <sup>44</sup> Department of Physics, Harvard University, 17 Oxford St, Cambridge, MA 02138, USA
```

Department of Astronomy, Harvard University, 60 Garden St, Cambridge, MA, 02138, USA
 Department of Astrophysical Sciences, Princeton University, Princeton, NJ 08544, USA
 Miller Institute for Basic Research in Science, 468 Donner Lab, Berkeley, CA 94720, USA
 Received 2025 May 10; revised 2025 August 8; accepted 2025 September 3; published 2025 September 29

Abstract

We present the La Silla Schmidt Southern Survey (LS4), a new wide-field, time-domain survey to be conducted with the 1 m ESO Schmidt telescope. The 268 megapixel LS4 camera mosaics 32 2k × 4k fully depleted CCDs, providing a $\sim 20 \text{ deg}^2$ field of view with 1" pixel⁻¹ resolution. The LS4 camera will have excellent performance at longer wavelengths: in a standard 45 s exposure the expected 5σ limiting magnitudes in g, i, z are \sim 21.5, \sim 20.9, and ~ 20.3 mag (AB), respectively. The telescope design requires a novel filter holder that fixes different bandpasses over each quadrant of the detector. Two quadrants will have i band, while the other two will be g and z band with color information obtained by dithering targets across the different quadrants. The majority (90%) of the observing time will be used to conduct a public survey that monitors the extragalactic sky at both moderate (3 days) and high (1 day) cadence, as well as focused observations within the Galactic plane and bulge. Alerts from the public survey will be broadcast to the community via established alert brokers. LS4 will run concurrently with the Vera C. Rubin Observatory's Legacy Survey of Space and Time (LSST). The combination of LS4 +LSST will enable detailed holistic monitoring of many nearby transients: high-cadence LS4 observations will resolve the initial rise and peak of the light curve while less-frequent but deeper observations by LSST will characterize the years before and after explosion. Here, we summarize the primary science objectives of LS4 including microlensing events in the Galaxy, extragalactic transients powered by massive black holes or stellar explosions, the search for electromagnetic counterparts to multi-messenger events, and supernova cosmology.

Unified Astronomy Thesaurus concepts: Sky surveys (1464); Astrophysical black holes (98); Supernovae (1668); Gravitational wave sources (677); Hubble constant (758); Gravitational microlensing (672)

1. Introduction

The quest to map the sky at high precision and to great depths has resulted in an unprecedented proliferation of wide-field, optical time-domain surveys. The need for repeated observations to build depth results in the production of light curves even when the discovery of transients and variables is not the primary science objective of a given experiment. This push toward the time domain has been driven by a bevy of exciting new discoveries in the past ~two decades, including significant advances in multi-messenger astronomy with the discovery of an optical counterpart to a gravitational wave (GW) event (Abbott et al. 2017a) and new neutrino sources being associated with electromagnetic radiation (e.g., IceCube Collaboration et al. 2018a; Stein et al. 2021). The spread of time-domain surveys ranges from bespoke efforts on small aperture telescopes to study very specific phenomena to extremely large projects designed to study the cosmos both with the time variable information they capture and the very deep images they produce by combining individual exposures. This later strategy is best illustrated by the forthcoming Legacy Survey of Space and Time

Original content from this work may be used under the terms of the Creative Commons Attribution 4.0 licence. Any further distribution of this work must maintain attribution to the author(s) and the title of the work, journal citation and DOI.

(LSST; Ivezić et al. 2019) conducted by the Vera C. Rubin Observatory, which will provide a decade-long movie capturing the variability of faint sources in the southern hemisphere on timescales ranging from days to years.

Many past and on-going experiments have laid the foundation for LSST by characterizing the time-variable sky, albeit at shallower depths or more narrow areas. These projects include: the Optical Gravitational Lensing Experiment (OGLE; Udalski et al. 1992), the All-sky Automated Survey (ASAS; Pojmański 1997), Palomar-QUEST (Djorgovski et al. 2008), the Catalina Sky Survey (CSS. Larson et al. 2003) and its associated Catalina Realtime Transient Survey (CRTS; Drake et al. 2009), the Sloan Digital Sky Survey-II (SDSS-II; Frieman et al. 2008), Skymapper (Keller et al. 2007), the Panoramic Survey Telescope and Rapid Response System (Pan-STARRS/PS1; Kaiser et al. 2010), the Palomar Transient Factory (PTF; Law et al. 2009), the All-sky Automated Survey for Supernovae (ASAS-SN; Shappee et al. 2014), the Evryscope (Law et al. 2015), the Dark Energy Survey (DES; Dark Energy Survey Collaboration et al. 2016), the Asteroid Terrestrial-impact Last Alert System (ATLAS; Tonry et al. 2018), the Zwicky Transient Facility (ZTF; Bellm et al. 2019b), the Young Supernova Experiment (YSE; Jones et al. 2021), BlackGEM (Bloemen et al. 2016), and the Gravitational-Wave Optical Transient Observer (GOTO; Steeghs et al. 2022). These projects have developed new insights for sources as close as

⁴⁸ LSST-DA Catalyst Postdoctoral Fellow.

moving objects within our solar system to distant supermassive black holes (SMBHs) that are more than halfway across the visible Universe. Collectively, these efforts have motivated and influenced the design of future upcoming surveys.

In this paper, we present a new time-domain survey, the La Silla Schmidt Southern Survey (LS4). LS4 is designed to discover extragalactic explosions and variable sources within the Milky Way using the La Silla Schmidt telescope along with the LS4 camera (see Section 2). Unlike the time-domain surveys listed above, LS4 has been designed to run concurrently with LSST, providing incredible opportunities for synergy (Section 3.3). LS4 can survey wider areas at a higher cadence than LSST while also monitoring the bright transients that saturate the LSST detector, LSSTCam. These bright transients are especially valuable as they are the most amenable to spectroscopic follow-up and multi-wavelength investigations, and therefore have an outsized role in advancing our understanding of extragalactic explosions. Below, we summarize the technical details of the telescope and camera, outline the LS4 survey strategy, and discuss the science that LS4 can achieve on its own while also describing the results that will be possible by combining LSST observations with the LS4 survey.

2. Overview of the ESO Schmidt, LS4 Camera, and LS4 Transient Discovery Pipeline

LS4 will be conducted using the ESO 1 m Schmidt Telescope located at the La Silla Observatory in Chile. The LS4 partnership will lease the Schmidt from ESO for a five year period to conduct the survey. The development of the LS4 camera and survey operations are paid for via funds raised by the partnership. The ESO Schmidt has a long history of conducting wide-field surveys, most recently as part of the La Silla-QUEST Survey (Rabinowitz et al. 2012; Baltay et al. 2013), and LS4 will build on that legacy.

2.1. The LS4 Camera

Full details of the LS4 camera and its performance are reported in K. Lin et al. (2025, in preparation). Briefly, LS4 leverages an upgrade to the QUEST camera (Baltay et al. 2007), which was used to conduct the La Silla-QUEST Survey, by replacing the detectors on the focal plane with 32 science-grade, 2k × 4k fully depleted CCDs that were fabricated for, but ultimately not installed on, the Dark Energy Camera (DECam; Flaugher et al. 2012). The 268 megapixel camera completely fills the Schmidt field of view (FOV), delivering $\sim 20 \text{ deg}^2$ images at a pixel scale of 1" pixel⁻¹. With the notable exception of the Kepler satellite (Borucki et al. 2010) and ZTF, LS4 has a larger étendue than any other timedomain survey with a similar aperture size as shown in Figure 1. The focal length of the telescope is 3 m, giving an f/3ratio. On nights with good seeing conditions, we expect a point spread function (PSF) full width at half maximum (FWHM) of \sim 2" (averaged over the field). Thus, at least 2 image pixels will typically cover the PSF core.

Each DECam CCD on the camera has two amplifiers located at two corners for a total of 64 amplifiers across the focal plane. Each CCD can be read out in two modes: dual amplifier (with a read-out time of \sim 17 s) and single amplifier (read-out time of \sim 34 s). When read out is in dual amplifier mode, six amplifiers fail to produce signal, reducing the overall FOV by \sim 9% (6/64). There is no room for a filter wheel within the telescope, and thus LS4 employs a novel design wherein four different parfocal filters, each covering a different quadrant of the camera, are affixed within the optical path of the detector. This design is illustrated in Figure 2, and at the start of the survey, there are two i-band filters, one g-band filter, and one z-band filter occupying the four quadrants.⁴⁹ During survey operations, color information will be obtained by dithering the telescope across different quadrants while pointing at the same locations in the sky. The LS4 filters were designed by Asahi Spectra using the same design as the filters being used with LSSTCam for LSST (the filter response curves are reported in K. Lin et al. 2025, in preparation). At the joints between two filters, approximately 2% of the total number of available imaging pixels will have "mixed light" with incident photons entering from multiple filters. 50 An additional few percent of the pixels will have reduced intensity due to a partial occultation of the beam by the filter holder, but this effect can be calibrated via flat fields. The pixels with mixed light will be read out from the detectors and stored in the database. The source detection pipeline will mask and ignore this region, though in principle a complex forward model could be constructed to search for transients on the affected pixels. The corners of the focal plane are also occulted by the edge of the field-flattener lens of the dewar, as illustrated in Figure 2, obscuring an additional $\sim 1.6\%$ of the total available pixels.

2.2. The Difference Imaging Detection Pipeline

Transients from LS4 will be detected in near real-time using the difference imaging pipeline SeeChange⁵¹ (see K. Lin et al. 2025, in preparation for additional details). The LS4 pipeline utilizes a "conductor," a component running on the National Energy Research Scientific Computing Center (NERSC) Spin kubernetes cluster (Snavely et al. 2018) that monitors files pushed from Chile to NERSC and tracks which images need to be processed.⁵² Processes running on the NERSC compute nodes will regularly contact the conductor to be assigned exposures to process. The pipeline splits an

⁴⁹ The LS4 collaboration also has an *r*-band filter, which could in the future be swapped in for any of the current filters in front of the focal plane.

⁵⁰ This effect is partially mitigated by the gaps in between the individual CCDs, see K. Lin et al. (2025, in preparation) for further details.

⁵¹ https://github.com/c3-time-domain/SeeChange

 $^{^{52}}$ When the internet goes down, data can be stored temporarily at the telescope on the 9 TB hard drive in the local storage computer (corresponding to \sim 30 nights of data).

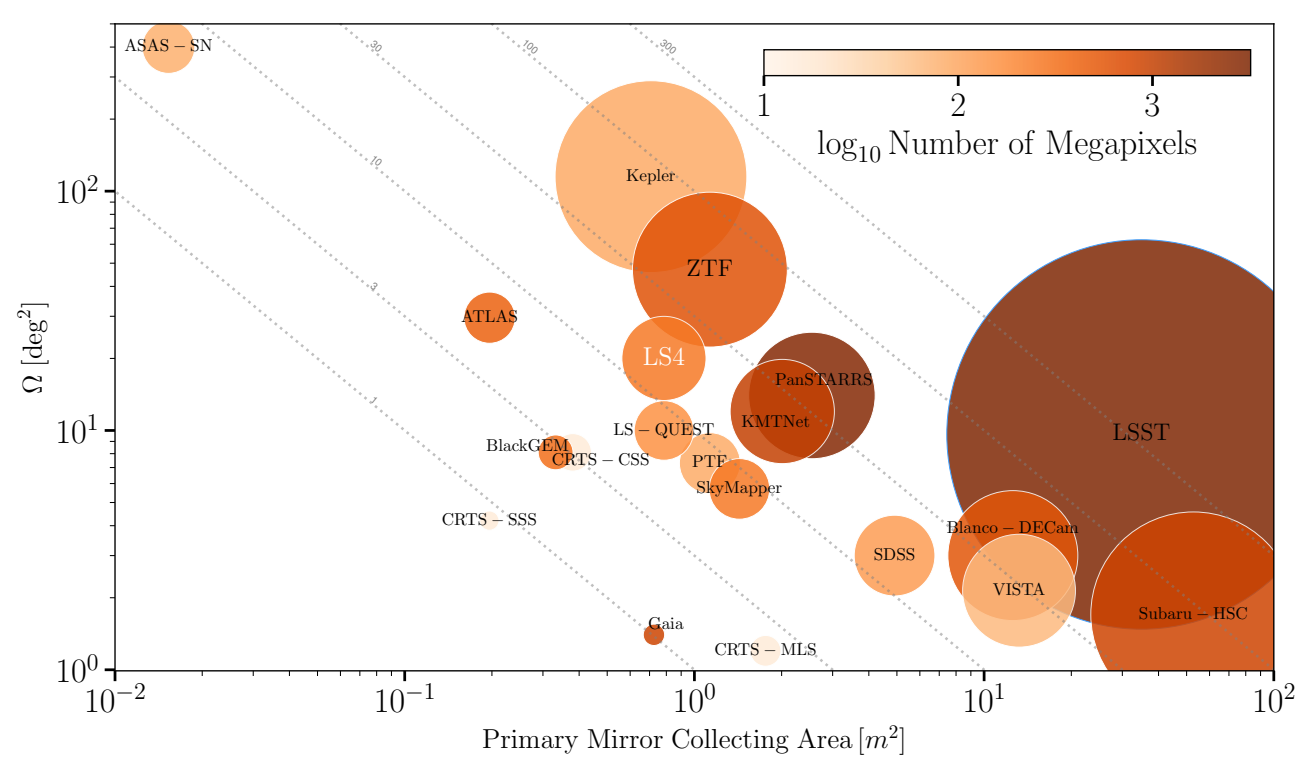


Figure 1. A comparison of the FOV (Ω) and light collecting area of the primary mirror (A) highlighting the étendue $(A\Omega)$ of past, current, and future time-domain surveys. The radius of the symbols is proportional to the étendue while the color corresponds to the total number of megapixels for the system. For surveys that employ multiple telescopes (ASAS-SN, ATLAS, Gaia, KMTNet, and PanSTARRS), the primary mirror collecting area is reported for a single telescope, while the FOV corresponds to the FOV of a single unit multiplied by the total number of telescopes (i.e., the figure reflects the optimistic scenario that every telescope is operational simultaneously). Dashed lines of constant étendue are shown along the diagonal. Among 1 m class telescopes, LS4 has a larger étendue than all but Kepler and ZTF.

exposure into its individual CCDs and launches parallel processes (one for each CCD) to simultaneously process all the CCDs. Standard procedures are used to identify variables and transients: pre-processing (overscan correction, flat fielding, etc.), source extraction, PSF estimation, astrometric calibration, photometric calibration, the subtraction of a reference image, and finally, residual identification. Preliminary cuts are applied to all residuals in the subtraction image, for example to eliminate dipoles, by removing sources that are nearly a 50/50 mix of positive and negative flux, and to eliminate residuals that are substantially different from the PSF. Only detections that pass these cuts and are above a signal-to-noise ratio threshold are saved. For the saved detections, SeeChange then creates 51×51 pixel thumbnails of the science, template, and difference images around surviving detections, and runs these thumbnails through the RBbot (N. Rehemtulla et al. 2025, in preparation) to produce a real/bogus score (see e.g., Bloom et al. 2012) between 0 and 1.

The pipeline generates alerts for all candidates that pass the preliminary filters (see K. Lin et al. 2025, in preparation for the full details). One alert encapsulates one detection. The alert schema⁵³

are based on, but modified from and greatly stripped down from, LSST alert schema. Alerts include basic image metadata (time of the exposure, filter, measurement of the seeing, measurement of the limiting magnitude), flux measurements, the real/bogus score, 51 pixel thumbnails around the detection from the science, template, and difference images, and summaries of any previous detections by the pipeline of a transient at the same position on the sky. The pipeline is capable of distributing alerts to multiple kafka servers. Public alerts from LS4 will be distributed through SCiMMA, ⁵⁴ which will sit upstream from the alert brokers ⁵⁵ and individuals that will ingest LS4 alerts.

For initial object subtraction, astrometric solution, PSF estimation, image alignment, and reference coaddition, SeeChange by default uses the Astromatic tools SExtractor, SCAMP, and Swarp (Bertin & Arnouts 1996). Image subtraction currently uses either the ZOGY (Zackay et al. 2016) or Alard/Lupton (Alard & Lupton 1998)

⁵³ https://github.com/c3-time-domain/SeeChange/tree/ls4_production/share/avsc

⁵⁴ https://scimma.org

⁵⁵ Alert brokers are systems that ingest "raw" alerts of variables/transients from time-domain surveys, filter the alerts based on user-supplied criteria while also adding information (e.g., from external catalogs or machine learning models), before distributing the annotated alerts to the broader community (see Nordin et al. 2019; Smith et al. 2019; Förster et al. 2021; Matheson et al. 2021; Möller et al. 2021, for examples and further details).

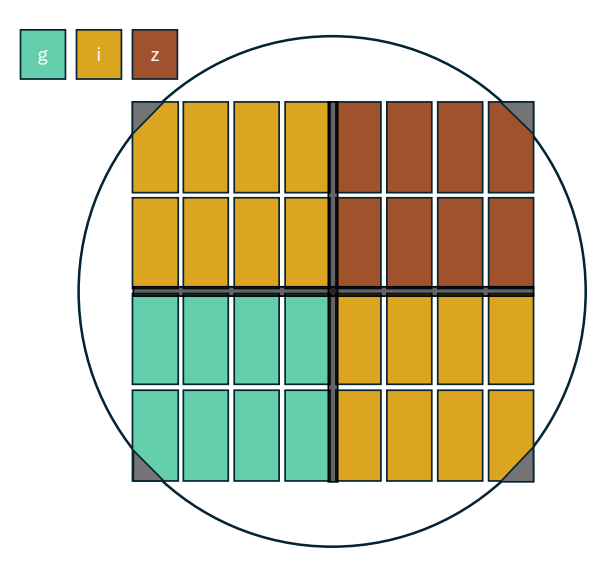


Figure 2. A schematic of the LS4 filter design on the CCD focal plane. The 32 CCDs are represented by the rectangles arranged in an array and shaded according to the filter that they are beneath at the start of the survey. The dark gray shaded regions that intersect at the center of the focal plane represents the occultation effect of the filter tray, affecting the pixels at the edges of the CCDs sitting at the filter joints. The detectors located at the corners are partially occulted by the edges of the field-flattener lens, which is outlined as the circle.

algorithms. Astrometric solutions and photometric calibration are both performed relative to Gaia DR3 stars (Gaia Collaboration et al. 2023).

From its inception, SeeChange has been designed with the capability of tracking multiple and different versions of the same data products. We anticipate a need for multiple versions due to software updates (e.g., bug fixes, new features, etc.), and users wanting to test different choices (e.g., the Alard/ Lupton versus the ZOGY subtraction algorithm). In the database, rows that keep track of data products (e.g., images, world coordinate solutions, zero-points, difference images, lists of detections on a difference image, measurements of those detections, etc.) have a provenance id column. A provenance is defined by several things: (i) the name of the process that produced it (e.g., image reduction, subtraction, detection, real/bogus estimation, synthetic source injection); (ii) the version of that part of the code; (iii) the parameters used (which can include the algorithm, for example for image subtraction); and (iv) the upstream provenance. As an example, for detection of residuals on a difference image, the provenance of the image subtraction used to create that difference image would be the upstream provenance. The provenance id is created as a hash of all of the values that define the provenance. As such, while known provenances are stored in the database, the code may create the provenance id directly without referencing the database. Including the upstream provenance id as part of a given step's provenance means that if an early step is changed (e.g., something in the

basic image reduction), then all downstream data products that could be affected by this change will have a different provenance.

When the SeeChange pipeline runs, it uses the version of its code and its configured parameters to figure out the provenance ids for all steps to be run. The pipeline queries the database at each step to see if a data product for that provenance already exists; if so, then the product is loaded. Otherwise, the pipeline performs the work necessary to create the data product, and then saves it to the database and the file store. Users interact with provenances through SeeChange "provenance tags," which are user-readable strings (including, for example, "default"). The database associates a provenance tag with a single provenance id for each process. Thus, a single provenance tag defines a unique set of data products given an initial on-sky (or simulated) exposure. This does add complexity when constructing direct SQL queries to the database, as such queries must make sure to filter data products based on the provenance, and (if using a provenance tag) to join properly to the provenance tag table. However, the See-Change web API will take care of constructing most of the necessary SQL queries behind the scenes. The interactive web application also includes a provenance browser that lets the user see all provenances associated with a given provenance tag, including the code version and all defined parameters for that provenance.

Ultimately, these design choices for SeeChange were made to ensure future flexibility in adjusting or testing new modules within the pipeline. Changes to the software or pipeline parameters will not require removing previous results from the database, or re-initializing the database. Users will be able to understand whether and why a specific transient was or was not detected while the survey was running, and analyses of detection efficiency will be able to ensure consistent processing where that is necessary.

3. The LS4 Survey

With its $\sim 20 \deg^2$ FOV, LS4 will conduct a rapid time-domain survey of the southern sky. As discussed in more detail below (see Section 4), the LS4 survey is designed to discover transients and variables while increasing the overall scientific output of the project by leveraging ongoing observations from other surveys that will also have coverage in the southern hemisphere, such as LSST ($m_{i,\text{lim}} \approx 24.0 \text{ mag}$; Bianco et al. 2022), ZTF ($m_{i,\text{lim}} \approx 19.8 \text{ mag}$; Bellm et al. 2019b), BlackGEM ($m_{i,\text{lim}} \approx 20.1 \text{ mag}$; Groot et al. 2024), ATLAS ($m_{o,\text{lim}} \approx 19.1 \text{ mag}$; Tonry et al. 2018), ULTRA-SAT ($m_{\text{NUV},\text{lim}} \approx 22.5 \text{ mag}$; Shvartzvald et al. 2024), the Ultraviolet Explorer (UVEX, $m_{\text{NUV},\text{lim}} \approx 24.5 \text{ mag}$; Kulkarni et al. 2021), and the Nancy Grace Roman Space Telescope ($m_{z,\text{lim}} \approx 25 \text{ mag}$; Akeson et al. 2019). The vast majority of the LS4 observing time (90%) will be used to conduct a public survey,

while the remaining 10% will be used by the LS4 collaboration for special projects.

3.1. The LS4 Public Survey

The LS4 public survey is primarily concentrated away from the Galactic plane to maximize the discovery of extragalactic transients and variables. Extragalactic fields are selected to have Galactic latitude $|b| \geq 10^{\circ}$ and $E(B-V) \leq 0.1$ mag, though in some instances visibility or lunation constraints may require observations of fields that do not satisfy these criteria. Approximately 1/4 of the public survey will be devoted to fields with high stellar density to search for variable stars and transient events, such as microlensing (see Section 3.1.3 for further details). Thus, the LS4 public survey is divided into three major campaigns covering (i) a wide area of the extragalactic sky, (ii) a small area to be observed at a higher cadence, and (iii) the Galactic plane. All observations from the public survey will be automatically processed and distributed to alert brokers for use by the community.

3.1.1. The LS4 Long-cadence ExtraGalactic Survey

Roughly 50% of the public survey will be devoted to the LS4 Long-cadence ExtraGalactic (LEG) Survey. The LEG Survey will monitor, on average, a $\sim 7000 \text{ deg}^2$ area with a 3 days cadence in the g, i, and z filters. Fields within the LEG footprint will be observed twice per night with a minimum \sim 30 minutes separation between images to identify and reject solar system moving objects from the extragalactic transient alert stream. Following the success of the ZTF Northern Sky Survey (Bellm et al. 2019a), the dual nightly visits will be conducted in different filters by shifting the telescope pointing by half the FOV between visits. On a given night, a source will be observed in either the g and i filters or the i and z filters, and when the field is revisited 3 days later, it will be observed with the opposite filter complement (i.e., the 3 days cadence refers to revisit time in the *i*-band). LS4 LEG will actively monitor both "high season" and "low season" LSST fields, once rolling observations of the Wide, Fast, Deep (WFD; Bianco et al. 2022) survey begin. LS4 LEG will discover and characterize long-lived transients over the entirety of the southern extragalactic sky.

3.1.2. The LS4 Fast Observations of Optical Transients (FOOT) Survey

Roughly 25% of the public survey will be devoted to the LS4 Fast Observations of Optical Transients (FOOT) Survey. LS4 FOOT will monitor, on average, a 1200 deg² area with a 1 day cadence using the same strategy as LS4 LEG, that is, observations will be collected in the *i*-band every night, while *g*- and *z*-band observations will alternate every other night. High-cadence LS4 FOOT observations will specifically focus

on rapidly evolving transients and primarily operate in LSST WFD "low season" fields. This observational strategy will ensure that Rubin captures very deep imaging in the year before (to search for pre-transient variability, e.g., Jacobson-Galán et al. 2020b) and the year after (to search for departures from "standard" radioactive decay, e.g., Graham et al. 2019) new LS4 FOOT discoveries are made.

Intrasurvey cadence between LS4, Rubin, and other public optical time-domain surveys (e.g., ATLAS and ZTF) covering the same footprint will enable a range of science cases covering intrinsically fast and young transients. By strategically obtaining LS4 observations on timescales of 1 day *after* scheduled Rubin observations, we will maximize the number of young transients whose rising light curves cross the threshold of LS4's ~21 mag limiting survey magnitude and guarantee detections in both surveys. This strategy has yielded several SN detections within 2 days of explosion in YSE using Pan-STARRS in conjunction with ZTF (see, e.g., Jones et al. 2021; Terreran et al. 2022; Aleo et al. 2023; Jacobson-Galán et al. 2024, and references therein), and the increase in survey volume from LS4 and Rubin can expand on these results.

3.1.3. The LS4 Stellar Oscillations, Lensing, and Eruptions Survey

The remaining ~25% of the public survey will be devoted to the LS4 Stellar Oscillations, Lensing, and Eruptions (SOLE) Survey. LS4 SOLE will target high-density star fields, primarily at low-galactic latitudes, in the plane between $-72^{\circ} \lesssim l \lesssim 36^{\circ}$ and $|b| \lesssim 4^{\circ}$, and in the bulge, from $|l| \lesssim 20^{\circ}$ and $|b| \lesssim 8^{\circ}$, to identify stellar transients (e.g., microlensing events) and variables. This ~1200 deg² Galactic plane region will be observed with a 1 day cadence in the *i*-band, with all fields cycling through g and g, similar to the LS4 LEG and LS4 FOOT surveys.

3.2. The Partnership Survey

One tenth of the LS4 observing time is reserved for the LS4 partnership. Alerts generated via observations from the partnership survey will only be released to the public after an expected proprietary period of $\sim \! 30 \, \mathrm{days}$. The fields to be observed and the time budgeted to them from the LS4 partnership survey are determined via an internal proposal process, and thus, the focus can change over time. At the start of survey operations, partnership observations will be primarily focused on observing fields that are regularly monitored by other surveys as well as follow-up of GW events discovered by LIGO-Virgo-KAGRA (LVK).

3.2.1. LS4 Deep Fields

Using partnership time, LS4 will co-observe the Euclid deep fields (Euclid Collaboration et al. 2022b) and the ULTRASAT

southern monitoring field. These observations will be conducted at a minimum cadence of 1 day, and form the basis for the LS4 deep fields survey. The LS4 FOV is especially well-matched to the Euclid Deep Field South (~23 deg²) and Euclid Deep Field Fornax (~210 deg²; see, e.g., Euclid Collaboration et al. 2022a, 2022b). LS4 observations will provide high-cadence monitoring of Euclid transients. Similar to Rubin, Euclid saturates for moderately bright sources (~17.8 mag), meaning LS4 will provide high-precision measurements for the brightest transients within the Euclid footprint. During the southern winter, ULTRASAT will spend >21 hr day⁻¹ staring at a single field to provide extremely high-cadence near-ultraviolet (near-UV) observations of a 204 deg² FOV near the southern ecliptic pole (Shvartzvald et al. 2024). LS4 will monitor this area with a 1 day cadence whenever it is visible.

3.2.2. Gravitational Wave ToOs

LS4 partnership target-of-opportunity (ToO) observations will be used to search the wide-area localizations for GW events discovered by LVK. LS4 ToOs for LVK events will be activated for new discoveries that meet the following criteria: (i) the LS4 search area is less than $1000 \, \mathrm{deg}^2$, which can include events with a localization $>1000 \, \mathrm{deg}^2$ if e.g., some of the localization area is in the north and will be observed by other facilities, (ii) the probability that the merger includes a neutron star $P(\mathrm{NS}) > 0.1$, and (iii) the false alarm rate is less than $1 \, \mathrm{yr}^{-1}$. Transient candidates identified via LS4 LVK ToO observations will be announced to the community via GCNs and TNS.

3.3. Synergistic Compatibility with LSST

The small aperture and large FOV of LS4 are particularly synergistic with the LSST WFD survey. In particular, LSST images will saturate for sources brighter than $r \approx 17.5 \,\mathrm{mag}$, meaning LS4 can "take over" monitoring any bright transients found by LSST that eventually saturate LSSTCam (only exceptionally nearby transients, like SN 2011fe, Nugent et al. 2011, will saturate LS4). Furthermore, the larger FOV of LS4 allows us to survey at a higher cadence than LSST, especially given the WFD goal to provide nearly uniform depth coverage across the entire southern sky in six different filters. LS4 fields will complement the "rolling cadence" to be implemented by WFD, whereby at any given time, roughly half of the visible WFD fields will obtain higher-cadence observations while the other half will be observed at a lower cadence (on average there are ~ 125 observations yr⁻¹ during "high season" and only \sim 25 observations yr⁻¹ during "low season"; The Rubin Observatory Survey Cadence Optimization Committee 2025). Highcadence LS4 FOOT observations will be primarily concentrated in WFD low-cadence regions to ensure that LS4 maximally fills the temporal gaps between LSST observations. In Figure 3 we show the simulated light curve of a normal Type Ia supernova (SN Ia) at z = 0.01, based on observations of SN 2011fe (Zhang et al. 2016), using version 4.3.1 of the baseline simulation of WFD from the Rubin Observatory (Yoachim 2025). We make the simplifying assumption that the seeing and cloud cover are perfectly correlated between La Silla, where LS4 is located, and Cerro Pachón, where Rubin is located, which is not completely unreasonable given the proximity of the two observatories. The sky noise for the simulated LS4 observations is scaled from the Rubin simulations by the difference in apertures and pixel scales. For the simulated light curves shown below (e.g., in Figure 3), the simulated transient is located at the arbitrary right ascension and declination $\alpha_{\rm J2000} = 00^{\rm h}$ 51′ 38″4, $\delta_{\rm J2000} = -22^{\circ}$ 32′ 24″0. This position is held constant for the different figures to illustrate the differing cadences depending on the LSST observing season.

As is clear from Figure 3, focusing LS4 FOOT survey observations in "low season" LSST fields provides high-cadence observations when transients are young and bright, the precise epochs when significant evolution occurs on short timescales. At the same time, WFD provides exceptionally deep observations (relative to LS4) in the year before and after the explosion with their own high-cadence observations that can constrain pre-explosion eruptions (e.g., Jacobson-Galán et al. 2022a) or monitor the late-time decay (e.g., Graur 2019) of LS4 FOOT discoveries. Together, LS4 and LSST will systematically monitor the very early and very late evolution of hundreds of new transients.

3.4. Multi-resolution Scene Modeling for Characterization of LS4 Transients

LS4 will additionally leverage higher resolution imaging from LSST and other telescopes to characterize transients with a full scene modeling approach (e.g., Holtzman et al. 1995; Brout et al. 2019), whereby the transient, the host galaxy, and background galaxies are forward modeled across multi-epoch imaging, enabling a measurement of the transient flux without the need for image differencing. This can be beneficial when combining photometry from multiple surveys without concern for reference image mismatch, measuring relative transienthost nucleus spatial offsets to classify sources as nuclear or non-nuclear, obtaining carefully sampled posteriors for transient and host galaxy parameters, and producing forced photometry of a faint source where the position is not wellconstrained (Ward et al. 2025). Given the 1.0 pixel scale and shallow depth of LS4, the inclusion of high-resolution and deeper images from Rubin or space-based imaging will significantly improve the forward model by resolving sources that are blended or undetected in LS4 imaging.

Joint analysis of LS4 and overlapping ZTF, Rubin, Euclid, Roman, or HST imaging can be done using new scene modeling codes such as Scarlet2: a new version of the Scarlet LSST deblender (Melchior et al. 2018) that can use both color and variability information to model variable point sources against a static background across multi-epoch, multi-

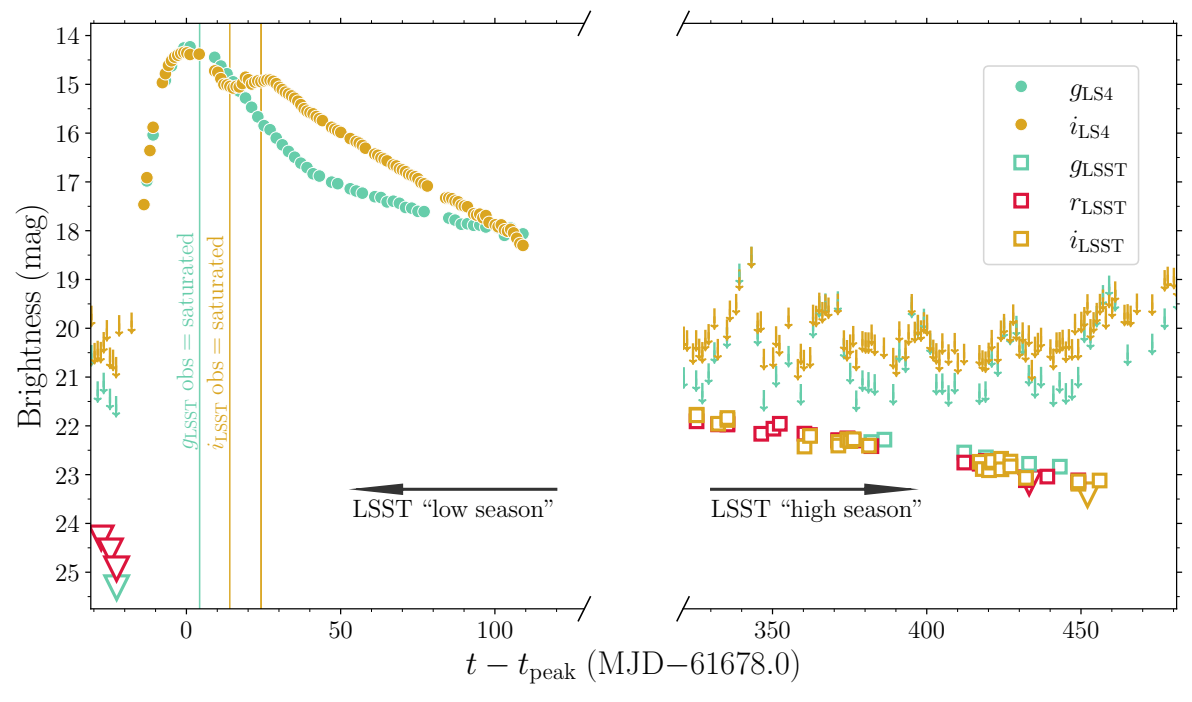


Figure 3. Simulated light curve of a Type Ia supernova based on observations of SN 2011fe (from Zhang et al. 2016) shifted to z = 0.01, which demonstrates the synergy between LS4 and LSST, especially after LSST begins rolling observations. The LSST WFD survey provides very deep limits a few weeks before $t_{\rm peak}$ and observations around peak brightness, but the limits are too early to constrain progenitor or explosion models and the maximum light observations are saturated. High-cadence LS4 observations place tight constraints on early emission and sample the rise and peak well. During the following observing season, ~ 1 yr after explosion, the SN is no longer detected by LS4 but LSST provides dense sampling to monitor the late-time decay as the field enters a WFD "high season." For clarity, uncertainties on the individual observations, as well as the LS4 z band and the LSST u, z, and y bands are not shown. LS4 upper limits are shown as downward facing arrows, while LSST upper limits are shown as downward facing triangles.

band, and multi-resolution imaging data. Scarlet2 provides the advantages of data-driven priors on galaxy morphologies enabling non-parametric galaxy models and is fully GPU compatible (Sampson et al. 2024; Ward et al. 2025).

In Figure 4 we show a key LS4 science application where multi-resolution forward modeling will be beneficial: modeling strongly lensed SNe across LS4, Rubin, and space-based imaging. Pixel-level simulations of the gravitationally lensed supernovae (gLSNe) population detectable by surveys like LS4 and Rubin show that the angular separations of most multiply imaged SNe will range from ~ 0.03 to 3.0 with a median of $\sim 0^{\prime\prime}.85$, such that most gLSNe will be unresolved or marginally resolved (Goldstein et al. 2019). When LS4 provides the high cadence photometry required to extract precise time delays from multiply imaged SNe for cosmography, a joint modeling framework will enable us to extract light curves from the poorly resolved systems without the need for a reference image. In another key science application, we will apply multi-resolution scene modeling to measure transient-host spatial offsets, assisting in distinguishing between nuclear and non-nuclear transients, and enabling the identification of spatially offset Tidal Disruption Events (TDEs) from wandering Massive Black Holes (MBHs), as demonstrated in Yao et al. (2025). Finally, we will use Scarlet2 to produce multi-survey light curves for transients that are present in reference imaging, including Active Galactic Nuclei (AGN), as demonstrated in Ward et al. (2025).

4. LS4 Science Working Groups

The analysis of LS4 observations within the collaboration will be conducted by five science working groups (SWGs): (i) Massive Black Holes, which focuses on TDEs, AGN, and other nuclear flares from the center of galaxies, (ii) Physics of Stellar Explosions, focused on core-collapse and thermonuclear SNe, (iii) Multi-messenger Astrophysics, focused on the search for electromagnetic counterparts to GW and neutrino detections, (iv) Cosmology, which will use SNe to study the expansion of the Universe, and (v) Galactic Transients and Variables, focused on stars within the Milky Way. In the sections below we highlight a non-exhaustive list of the science that will be pursued by the individual LS4 SWGs.

5. Massive Black Holes

5.1. Using TDEs to Probe MBH Accretion and Jet Physics

When a star passes too close to an MBH, it can be shredded by tidal forces and subsequently accreted (Rees 1988;

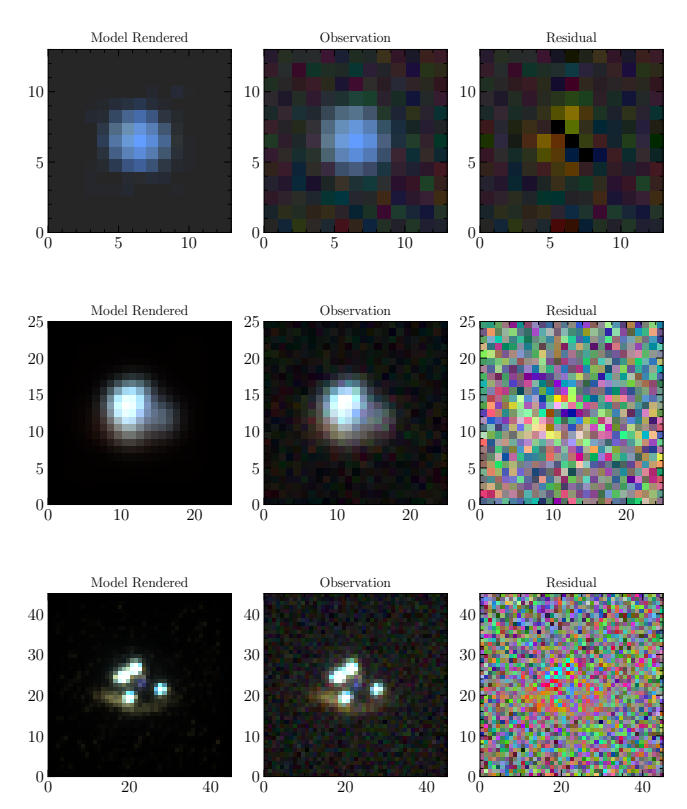


Figure 4. Example Scarlet2 rendered models, observations, and residuals for a gravitationally lensed, quadruply imaged SN jointly modeled across simulated LS4 (top), Rubin (middle), and Roman (bottom) imaging. We show a 13" by 13" cutout of the LS4 image, and a 5" by 5" cutout of the corresponding Rubin and Roman images. The system is unresolved in LS4 imaging, partially resolved in Rubin imaging, and well-resolved in space-based Roman imaging. Joint analysis with a higher resolution image enables extraction of an LS4 light curve of each SN image in the system.

Gezari 2021), producing a flare visible from the X-rays to the radio band. These TDEs produce a similar luminosity to SNe in the optical and UV, but they are intrinsically rare. The TDE rate in Milky Way like galaxies is $\sim 3 \times 10^{-5} \text{ yr}^{-1}$ (Yao et al. 2023). Persistent blue optical colors and a long-lasting plateau distinguish TDEs from SNe, though the duration of their peak optical emission is similar to core-collapse supernovae (CCSNe), $\sim 20-100$ days. A small fraction of TDEs launch relativistic on-axis jets, which can produce a fast transient with an early-time red peak in the optical (Andreoni et al. 2022a).

TDEs provide a laboratory to study the real-time formation and evolution of MBH accretion flows (Wevers et al. 2021; Yao et al. 2022, 2024a), as well as particle acceleration and energy dissipation in newly launched jets (Burrows et al. 2011; De Colle & Lu 2020; Yao et al. 2024b). Multi-wavelength observations are crucial for future progress, but follow-up campaigns can only begin once a TDE has been discovered. There are few optical TDEs with a well-characterized rise and peak, but high-cadence surveys, such as LS4, will discover more events during this critical phase.

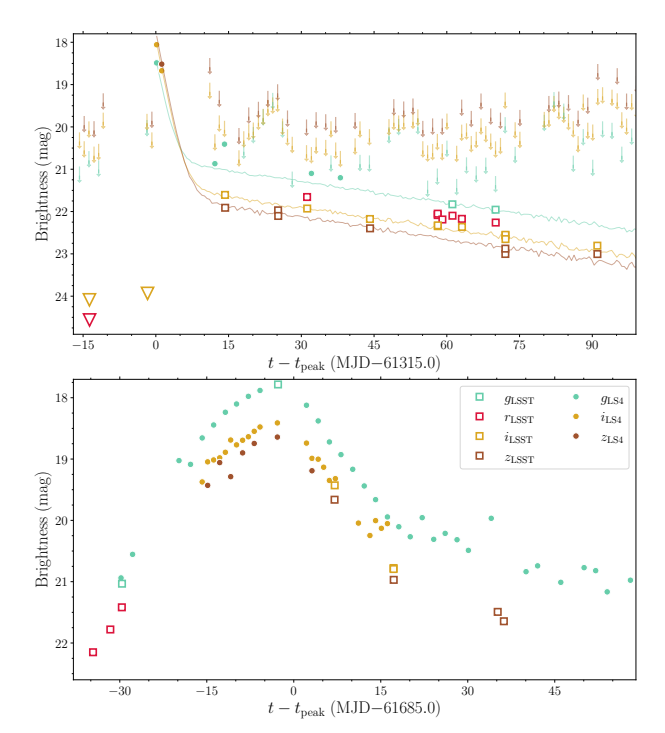


Figure 5. Simulated TDE light curves as observed by LS4 and LSST. Top: a jetted TDE at z=0.9, using the SED model of AT 2022cmc (Hammerstein et al. 2025), which is the only known jetted TDE discovered in the optical (Andreoni et al. 2022a). The initial rapid decay is captured in LS4 FOOT survey observations and missed by LSST, which nevertheless continues to detect the transient for several months after it fades below the LS4 detection limit. The thin solid lines show the evolution of the TDE model. Bottom: simulation of a low-luminosity TDE that lacks a jet at z=0.027, based on the optical evolution of AT 2020wey (Yao et al. 2023). LSST has extremely sparse observations around the peak of the TDE, but plays an essential role in characterizing the shape and duration of the rising portion of the light curve. For clarity LS4 upper limits are not shown in the bottom panel of this figure. In both the top and bottom panel, symbols and markers are the same as Figure 3.

High-cadence *i*- and *z*-band observations from LS4 offer a unique opportunity to identify jetted TDEs because the early-time synchrotron spectrum is brighter in these filters than the *g* band (see Figure 5, upper panel). Following discovery, LSST will monitor the much fainter long-lasting thermal component. For non-jetted TDEs, LSST can provide very early detections (see Figure 5, lower panel), to constrain the photometric rise.

5.2. Using TDEs to Probe MBH Demographics

TDE population studies can address fundamental open questions about MBH demographics. The formation of the very first BHs in the Universe remains unclear. Leading hypotheses suggest that they formed either through the core collapse of Population III stars, which produce BHs with masses of $\sim 10^2 M_{\odot}$ (light seeds), or through the direct collapse of gas clouds, which form more massive BHs around $\sim 10^5 M_{\odot}$ (heavy seeds). Local dwarf galaxies, with their relatively quiet star formation and merger histories, exhibit similarities to

high-redshift galaxies. Therefore, the fraction of local dwarf galaxies that host central BHs—referred to as the occupation fraction, $f_{\rm occ}$ —provides insights into early BH seeding mechanisms. Light seed models, for example, predict higher values of $f_{\rm occ}$ (Greene et al. 2020).

The volumetric rate of TDEs in dwarf galaxies offers a unique way to estimate $f_{\rm occ}$. However, past blue-optical sky surveys have been limited in detecting TDEs in these galaxies because (1) most TDE experiments select transients in known galaxy centers, but dwarf galaxies are highly incomplete in catalogs, and (2) TDEs powered by lower-mass BHs might be intrinsically fainter in the blue-optical bands relative to the i and z bands. LS4+LSST can address these challenges. Deep LSST imaging will detect very low-mass host galaxies ($\sim 10^7 \, M_\odot$) and monitor TDEs long after they fade below the LS4 detection limit. LS4 will provide high-cadence data during the peak of the light curves, facilitating the selection of TDE candidates.

5.3. Physics of TDE Optical Emission

The UV and optical ($\lambda \lesssim 1~\mu m$) emission from TDEs imply emitting regions that are much larger and cooler than expected for accretion disk emission at the tidal radius. Either X-rays from the accretion disk are being reprocessed by outflows (Dai et al. 2018; Lu & Bonnerot 2020) or an alternative model, such as shocks produced in the intersection of the debris stream (Piran et al. 2015; Huang et al. 2024), is needed to explain the observed emission.

While it is widely accepted that TDE light curves encode the properties of the disrupted star and the mass of the disrupting BH-parameters that define physical dimensions and timescales for the TDE—current light curve fitting methods rely on assumptions about the power sources and emission processes that are still uncertain. For instance, BH mass estimates derived from light curve fitting sometimes conflict with values inferred from galaxy scaling relations (e.g., Hammerstein et al. 2023b; Ramsden et al. 2025); and some events exhibit multiple distinct peaks in their optical light curves that cannot be explained with a single process/energy ejection (Ho et al. 2025). Furthermore, some TDEs show broad H, some show broad He, some show both, and some show neither (van Velzen et al. 2021; Hammerstein et al. 2023b). The origin of these features and the physical distinction between these classes are not yet well understood.

5.4. Early Light Curves and Late-time Plateaus

Early bumps (e.g., AT 2023lli, AT 2024kmq; Huang et al. 2024; Ho et al. 2025), blips, and changes in slope in the rising phase (e.g., AT 2019azh, AT 2020zso; Faris et al. 2024; Guo et al. 2025) of optical TDEs encode the outflow physics and suggest more than one dominant emission mechanism contributes to the pre-peak light curve. High-cadence LS4

observations will be critical for constraining TDE emission models, ultimately enabling TDEs to serve as a reliable probe of MBH properties.

Several recent studies have shown that the UV/blue-optical light curves for a large fraction of TDEs flatten at late times (van Velzen et al. 2019; Mummery et al. 2024). The plateau originates as the viscous spreading of the disk competes with the cooling of the disk as the accretion rate declines. Fitting these late-time observations to relativistic accretion disk models shows that the plateau luminosity correlates with the central BH mass, as estimated from host galaxy properties. LSST will detect these late-time plateaus for LS4-discovered TDEs, providing an independent probe to measure the mass of the central MBH.

5.5. TDE Host Galaxies

Theoretical work has suggested that TDE rates are enhanced in galaxies with asymmetric stellar distributions, which produce torques that drive stars toward the nucleus (Stone et al. 2020). Whether such predictions are borne out is difficult to determine: TDE samples are complicated by the confluence of diverse host galaxy stellar populations and dynamics, unknown levels of dust obscuration, and the unknown role of pre-existing nuclear activity (French et al. 2020).

Current observational work has shown that TDE rates may also be enhanced in galaxies with post-starburst, or E+A, stellar populations (Arcavi et al. 2014; French et al. 2016; Law-Smith et al. 2017; Hammerstein et al. 2021). The precise reason for this enhancement is not known, but the possible post-merger nature of these galaxies may be responsible for the boost in the TDE rate (Stone & Metzger 2016; Stone & van Velzen 2016; Hammerstein et al. 2021, 2023a). Uncovering the true enhancement of these galaxies in TDE populations is key to understanding the mechanisms by which TDEs are triggered, and this can only be done with a larger sample of TDEs. As described in Section 3.4, deep LSST imaging will enable detailed studies of the host morphologies and spectral energy distributions of LS4 TDEs.

5.6. Irregular (and Regular) AGN Variability

LS4+LSST will improve the time-sampling and spectral coverage of AGN to probe variations in accretion or jet activity with unprecedented precision (e.g., LSST Science Collaboration et al. 2009). This census will help define "outliers," such as rare changing-look AGN (CLAGN; e.g., MacLeod et al. 2016; Ricci & Trakhtenbrot 2023), turn-on activity (Gezari et al. 2017; Nyland et al. 2020; Sánchez-Sáez et al. 2024) and narrow-line Seyfert 1-related transients (Frederick et al. 2021). An important emerging result is that the disks in these variable AGN appear to change accretion modes faster than would be expected from the thin-disk viscous timescale. The LS4 LEG and FOOT surveys will make

key progress in understanding these rarities by discovering them on the rise.

Periodic variations in AGN light curves can reveal binary MBHs situated at the center of AGN (e.g., Graham et al. 2015a, 2015b; Charisi et al. 2016; Liu et al. 2016; Li et al. 2023). High-resolution Very Long Baseline Interferometry (VLBI) can spatially resolve only low-redshift binary AGN (e.g., Rodriguez et al. 2006) or larger separation dual AGN (e.g., Veres et al. 2021), whereas long-term photometric monitoring can reveal small separation AGN binaries. The multi-year duration of LS4 will enable the search for long-term periodicities in AGN light curves.

5.7. Other Nuclear Transients

Galactic nuclei also play host to other time-variable phenomena, including extreme AGN flares and nuclear SNe. In particular, "Ambiguous Nuclear Transients" (ANTs; Holoien et al. 2022) and "Bowen Fluorescence Flares" (BFFs; Trakhtenbrot et al. 2019b) have blurred the line between TDEs and extreme AGN accretion episodes, requiring larger samples to determine their origins.

ANTs exhibit properties of both TDEs and AGN, with some occurring in previously inactive galaxies. Their light curves resemble TDEs but evolve more slowly, last hundreds of days, and often reach higher luminosities $(L_{\text{peak}} \gtrsim 10^{44} \, \text{erg s}^{-1})$, although some are fainter (e.g., AT 2018zf and AT 2020ohl, Trakhtenbrot et al. 2019a; Ricci et al. 2020; Hinkle et al. 2022, 2023; Laha et al. 2022). Their radiated energy $10^{51} \lesssim E \lesssim 10^{53}$ erg (Subrayan et al. 2023; Wiseman et al. 2023, 2025) makes some of them (so-called "Extreme Nuclear Transients" or ENTs) the most energetic long-lived transients in the Universe. Many ANTs show mid-IR flares and UV/ optical/IR emission consistent with dust sublimation, suggesting reprocessed light from a dusty torus (Jiang et al. 2017b; Petrushevska et al. 2023; Hinkle 2024; Oates et al. 2024). LS4 will efficiently detect new ANTs and ENTs, enabling studies of whether they arise from novel AGN accretion modes, massive TDEs, or spinning MBHs. LS4 z-band observations will also track the blue tail of mid-IR flares, offering insights into ANT emission mechanisms.

BFFs are a recently discovered class of accreting MBHs, characterized by steep-rise, slow-decline optical flares, bright UV and radio emission, and AGN-like spectra with emission lines driven by Bowen fluorescence (Bowen 1934). Their flares persist for ~1 yr, sometimes with secondary flares, and may represent TDEs occurring within AGN disks (Veres et al. 2024). High-cadence LS4 observations will capture BFFs on the rise, while combined LS4+LSST data will track their decline and color evolution, distinguishing them from standard AGN variability.

5.8. Classification and Follow-up Efficiency

Low-level AGN variability detected by LSST can rule out "normal" AGN activity and reduce contamination in samples of TDEs and other unusual accretion events found by LS4. To spectroscopically classify TDEs and other nuclear transients we will use the ESO 4 m Multi-Object Spectroscopic Telescope (4MOST; de Jong et al. 2019) multi-object spectrograph, which will classify >10⁵ transients (including nuclear ones) as part of the Chilean AGN/Galaxy Extragalactic Survey (ChANGES; Bauer et al. 2023) and Time Domain Extragalactic Survey (TiDES; Frohmaier et al. 2025) campaigns, Son of X-Shooter (SoXS; Schipani et al. 2018), SDSS-V (Kollmeier et al. 2019), the Dark Energy Spectroscopic Instrument (DESI; DESI Collaboration et al. 2016), and Las Cumbres Observatory (LCO; Brown et al. 2013), where dedicated programs are already in place.

6. Physics of Stellar Explosions

The vast majority of extragalactic transients found by LS4 will be SNe, which will provide a significant opportunity to advance our understanding of the explosions that punctuate the end of some star's lives. In the past decade, PTF, Pan-STARRS, and ZTF have demonstrated that a combination of very early, multi-color detections and long observational baselines, both before and after the explosion, can provide unique insights into the nature of SNe that are not possible when limited to maximum light photometry/spectroscopy (e.g., Soderberg et al. 2004; Mauerhan et al. 2013; Graur et al. 2016, 2020; Jacobson-Galán et al. 2018, 2020b; Terreran et al. 2022; Tsalapatas et al. 2025). As noted in Section 3.3, LS4 +LSST will build on this legacy while uniquely probing the years before and after explosion to unprecedented depths for thousands of SNe. This will provide the global SN community ample time to trigger critical follow-up observations, including high-resolution spectroscopy, infrared imaging and spectroscopy, spectropolarimetry, and X-ray and radio follow-up. Below we highlight some of the most interesting science cases that can be pursued with LS4 alone, as well as the synergistic power of combining LS4 with LSST.

6.1. Infant Core-collapse Supernovae

The LS4 FOOT survey (see Section 3.1.2) is designed to routinely discover SNe within 48 hr of first light. Such discoveries require rapid vetting and follow-up. Latencies in vetting and follow-up remain a major bottleneck in infant transient studies, but automation can reduce the time lag. In its alert stream, LS4 will employ image-based deep learning for young transient identification. Building from the success of BTSbot (Rehemtulla et al. 2024), which identifies ZTF alerts that originate from bright ($m_{\rm peak} < 18.5$ mag) extragalactic transients, LS4 will integrate alert streams from multiple

surveys to increase the rate of these discoveries. By incorporating autonomous transient identification and follow-up tools (e.g., Rehemtulla et al. 2025), LS4 will pursue similar no-human-in-the-loop automation, reducing follow-up latency from next night spectroscopy to minutes or hours.

Spectra of 1-2 days old SNe guarantee a rich vield of transient emission and absorption features. Numerous studies have shown that a large fraction of CCSNe are engulfed in compact ($\sim 10^{14}$ cm) shells of circumstellar material (CSM) that is swept up by the SN ejecta within days of explosion (e.g., Bruch et al. 2021, 2023; Jacobson-Galán et al. 2024). In response to the radiation field of the SN shock break-out, this CSM is excited and ionized, producing a series of recombination lines that can be visible for several days. As demonstrated by the analysis of "flash spectroscopy" data (Niemela et al. 1985; Gal-Yam et al. 2014; Yaron et al. 2017), the spectral lines that appear following the excitation and ionization of the CSM encode information of the surface composition of the dying star just before it explodes (Groh 2014; Gal-Yam et al. 2022; Schulze et al. 2025), the mass-loss history of the progenitor star (Yaron et al. 2017; Boian & Groh 2020; Jacobson-Galán et al. 2024), and details about the SN shock propagation (Zimmerman et al. 2024). Together, these data enhance our understanding of what massive stars do just before they die and the SN explosion mechanisms themselves. Furthermore, combined with pre-SN imaging from LSST, reaching 2-3 mag deeper than previous surveys, this method can constrain the progenitor's mass-loss history over timescales of weeks, months, and years before the explosion (Ofek et al. 2014; Strotjohann et al. 2021; Jacobson-Galán et al. 2022a), offering an unprecedented window into the final evolutionary stages of massive stars.

6.2. The Mass-loss History of Dying Massive Stars

Hydrogen-poor CCSNe arise from massive stars that lose most or all of their hydrogen envelopes before core collapse. These SNe, collectively known as stripped-enveloped SNe (SESNe), include several subtypes (Filippenko 1997; Gal-Yam 2017): Type IIb SNe (which retain some hydrogen), Type Ib SNe (which lack hydrogen but contain some helium) and Type Ic SNe (which have neither hydrogen nor helium). Extensive studies of SESNe suggest that their low ejecta masses are inconsistent with their mass loss being driven solely by stellar winds (e.g., Taddia et al. 2015; Prentice et al. 2019), which favors a binary origin instead. However, if these SNe indeed result from binary interactions, they should be surrounded by a significant amount of CSM, with its mass and distribution likely influenced by the binary separation (Smith 2014).

Some SESNe exhibit multiple peaks in their early light curves, likely caused by the shock breakout at either the surface of the progenitor or through an extended envelope surrounding it (Woosley et al. 1994; Bersten et al. 2012;

Piro 2015). Large sample studies (e.g., Das et al. 2024) show that these events contribute between 3% and 10% of the SESN rate. The LS4 FOOT survey (Section 3.1.2) will allow us to measure the rate and properties of initial peaks for a large number of SN classes (e.g., IIb, Ib, Ic, Ic-BL) to improve our understanding of what massive stars do just before they die.

In recent years, an increasing number of SESNe have shown double-peaked light curves at later stages, likely caused by the interaction of the SN ejecta with CSM. In some cases, the SNe simultaneously show a spectroscopic metamorphosis into a CSM-powered SN (e.g., SN 2014C, Milisavljevic et al. 2015; SN 2017ens, Chen et al. 2018), whereas in others such a spectroscopic transformation is either subtle (SN 2022xxf, Kuncarayakti et al. 2023; SN 2022jli, Moore et al. 2023; Chen et al. 2024) or even absent (e.g., SN 2019tsf, Sollerman et al. 2020; SN 2019cad, Gutiérrez et al. 2021; SN 2023aew, Kangas et al. 2024; Sharma et al. 2024) despite a clear increase in optical (4000 Å $\lesssim \lambda \lesssim 9000$ Å) flux. The reasons for that are debated. Combining LS4 with LSST will allow us to monitor SN light curves for hundreds of days and, therefore, not only measure the rate and properties of rebrightenings but also how the rebrightenings evolve as a function of the light curve phase and SN type. Acquiring well-timed spectra provides the unique opportunity to gain a much-improved understanding of the physics of SN ejecta+CSM interaction, the pre-SN mass-loss episodes (stellar winds versus episodic outburst versus binarydriven envelope stripping; Smith 2014, Morozova et al. 2018), and ultimately about the uncharted late-stage evolution of dying massive stars.

Many interacting SNe exhibit rebrightenings, undulations and irregular declines (Nyholm et al. 2020), indicating the presence of clumpy, multi-shell, or asymmetric CSM structures. The LS4 FOOT survey will characterize these fluctuations from geometric asymmetries and density variations (Kiewe et al. 2012; Ofek et al. 2014), differentiating between steady mass loss and episodic/explosive ejections and uncovering the physics governing the CSM interaction processes (Moriya et al. 2013; Ofek et al. 2014; Khatami & Kasen 2024). Long-term monitoring, which will be provided by LS4+LSST, will uncover additional events like iPTF14hls (Arcavi et al. 2017a), which had a long-lived undulating light curve that was suggested to be powered by magnetars, fallback accretion, or CSM interaction. Only with observations collected several years after explosion would some of these scenarios be ruled out (Sollerman et al. 2019).

6.3. Engine-driven Transients

Engine-driven astronomical transients, a heterogeneous class, are powered by BHs and neutron stars (NSs). Examples include the recently discovered Fast Blue Optical Transients (FBOTs, e.g., Drout et al. 2014; Ho et al. 2022) and gamma-ray bursts (GRBs), which come from massive stellar explosions and

binary NS mergers. Engine-driven transients can launch relativistic outflows with a range of collimation properties, which is a consequence of the deep gravitational potentials of their compact objects. As a result, the electromagnetic evolution of these events evolves on shorter timescales than normal SNe. The LS4 FOOT survey is designed to capture the $\sim 1 \, \mathrm{day}$ timescales associated with engine-driven events.

A decade after the discovery of FBOTs (Drout et al. 2014), it is now clear that low-luminosity FBOTs represent the "tail" of already known phenomena (e.g., cooling-envelope emission from Type IIb SNe), and that Luminous FBOTs (LFBOTs hereafter) represent a physically distinct class of events (e.g., Ho et al. 2022). Reaching a peak luminosity $L_{\rm peak}\approx 10^{45}~{\rm erg~s^{-1}}$ in a few days, LFBOTs challenge models invoked to explain ordinary stellar explosions and require more exotic scenarios. While the intrinsic nature of LFBOTs is still highly debated (with interpretations ranging from jetted stellar explosions to TDEs on IMBHs), X-ray and radio observations of a handful of LFBOTs have led to the discovery of a rich phenomenology, including mildly relativistic ejecta (e.g., CSS 161010, Coppejans et al. 2020).

At the same time, GRB afterglows, which are powered by synchrotron emission with an $f_{\nu} \propto \nu^{-1}$ spectrum, are more luminous in the i and z band than g band. Thus, LS4, which is more sensitive in the i and z band than any other facility with a similar FOV, can play a critical role in expanding the phase space to discover "orphan afterglows" in the local Universe (i.e., GRB afterglows that eluded high-energy telescopes either because of satellite sensitivity or pointing at the time of the GRB), as well as GRB events for which the jet is intrinsically absent (e.g., choked by baryons like in baryon-loaded fireballs; Cenko et al. 2012).

6.4. Superluminous Supernovae

Hydrogen-poor superluminous supernovae (SLSNe-I; Quimby et al. 2011) are a rare $(5.6^{+5.4}_{-2.8} \,\mathrm{Gpc^{-3}\,yr^{-1}}; \,\mathrm{Perley})$ et al. 2020) class of transients that peak in the UV/blue-optical with absolute magnitudes between -23 and -20 mag. These enigmatic explosions are about a factor of 10-100 more luminous than ordinary CCSNe (De Cia et al. 2018; Lunnan et al. 2018a; Angus et al. 2019; Chen et al. 2023a). Despite recent observational breakthroughs (e.g., Nicholl et al. 2015, 2016; Yan et al. 2017a, 2017b; Bose et al. 2018; Lunnan et al. 2018b; Quimby et al. 2018), the underlying physical mechanisms that drive their extreme luminosities remain debated (Moriya et al. 2018; Gal-Yam 2019). They are thought to be powered by one of the following: the spin-down of a rapidly rotating young magnetar (Kasen & Bildsten 2010), interaction of the SN ejecta with a massive (3–5 M_{\odot}) C/O-rich CSM (Blinnikov & Sorokina 2010; Baklanov et al. 2015), pulsational pair-instabilities in which collisions between highvelocity shells are the source of multiple, bright transients (PPISNe; Woosley et al. 2007), or tidal disruption of the companion star by a compact object born in a binary system (Tsuna & Lu 2025).

Light curves are essential to understand the immense source of energy and progenitors of SLSNe. ZTF revealed photometric bumps and wiggles in a large number of SLSNe-I (Chen et al. 2023b, see also Hosseinzadeh et al. 2022), likely due to CSM interaction. The LS4 LEG Survey (Section 3.1.1) will capture similar variability in the giz light curves of many SLSNe-I ($z \lesssim 0.2$).

LSST WFD will supplement LS4 discoveries by capturing bumps on the rising portion of the SLSN light curve (luminosity: -16 to -20 mag; duration: $\leq 20-30$ days; Leloudas et al. 2012; Nicholl et al. 2015; Nicholl & Smartt 2016; Smith et al. 2016; Angus et al. 2019) or slowly rising plateaus before the "normal" rise (Anderson et al. 2018). Furthermore, while LS4 probes the photospheric phase, LSST will monitor SLSNe-I for 100s of days into the nebular phase. These latetime observations are very sensitive to the SLSN powering mechanism including magnetars and radioactive decay. Finally, deep LSST observations will be especially useful for identifying the faint, star-forming dwarf galaxies associated with SLSNe-I (Lunnan et al. 2014; Leloudas et al. 2015; Perley et al. 2016; Chen et al. 2017; Schulze et al. 2018). Detailed knowledge of the host galaxies has the potential to transform our understanding of the powering mechanisms, progenitors, and physics that operate within SLSNe.

LSST will discover thousands of SLSNe, but the sparse cadence in LSST WFD is insufficient to fit models and infer critical parameters like the ejected mass. In simulated LSST light curves SLSN model parameters could only be recovered 18% of the time (Villar et al. 2018). By resolving the light-curve peaks for hundreds of $z \lesssim 0.5$ SLSNe, LS4 will provide accurate measurements of the ejecta mass distribution to constrain SLSN progenitor models.

6.5. Early Observations of Type Ia Supernovae

Observations of SNe Ia shortly after explosion can strongly constrain theoretical predictions about the explosion mechanism. Resolved "bumps" in the early *g*- and/or *r*-band emission of several SNe Ia have been detected (e.g., Goobar et al. 2015; Hosseinzadeh et al. 2017; Jiang et al. 2017a; Dimitriadis et al. 2019; Shappee et al. 2019; Deckers et al. 2022; Srivastav et al. 2023). In addition, strong, early UV emission has now been detected in two SNe, iPTF 14atg (Cao et al. 2015) and SN 2019yvq (Miller et al. 2020; Burke et al. 2021; Tucker et al. 2021), though their subsequent evolution was very different. Multiple models could explain the early excess flux, including shock interaction with a non-degenerate companion star (Kasen 2010), helium shell burning in the double-detonation of a sub-Chandrasekhar mass white dwarf (Shen et al. 2018; Polin et al. 2019), CSM interaction (Piro &

Morozova 2016), or the presence of radioactive ⁵⁶Ni in the outer ejecta (Piro 2012; Magee & Maguire 2020). The LS4 FOOT survey combined with advances in the autonomous identification of infant SNe will allow us to routinely discover infant SNe Ia and swiftly obtain critical follow-up observations (see also Section 6.1).

6.6. Intrinsically Red and Dust-obscured Stellar Explosions

The frequency and depth of LS4 i- and z-band observations provide a unique opportunity to search for exceptionally red stellar explosions, an area that is historically underexplored. Recent discoveries demonstrate that some exotic explosive events have intrinsically red optical colors ($g - i \gtrsim 1$ mag), including a new class of peculiar SNe Ia thought to be associated with sub-Chandrasekhar mass white dwarf (WD) progenitors (Jiang et al. 2017a; De et al. 2019; Liu et al. 2023b) as well as a variety of underluminous "gap" transients (Munari et al. 2002; Tylenda et al. 2011). Similarly red-optical colors are also observed in normal SNe (especially some SESNe), often due to extrinsic factors such as line-of-sight extinction from their dusty stellar nurseries. LS4 will be proficient in hunting these red transients, which are systematically missed in surveys optimized for the blue-optical.

Extreme line blanketing from iron-group elements (IGEs) in the maximum-light spectra of SNe Ia provide strong evidence for the helium-shell double-detonation explosion of a sub-Chandrasekhar mass WD (e.g., Polin et al. 2019). After a brief flash powered by radioactive decay, the IGEs formed in the helium-shell detonation will obscure most of the UV and blue-optical ($\lambda \lesssim 5000$ Å) flux from the SN, leading to a dramatic blue-red color inversion on the rise and/or an exceptionally red color ($g-r \gtrsim 0.75$ mag) at peak (e.g., Noebauer et al. 2017; Polin et al. 2019). Several candidate double-detonation explosions have been found (e.g., Jiang et al. 2017a; De et al. 2019; Dong et al. 2022; Liu et al. 2023a, 2023b; Padilla Gonzalez et al. 2023), and the i- and z-band observations of LS4 will readily identify the pronounced flux suppression seen in these SNe.

Some massive stars produce red transients that fall in the nova-SN luminosity "gap" (Kasliwal et al. 2011), such as luminous red novae (LRNe) and intermediate luminosity red transients (ILRTs). LRNe are usually associated with binary stars that have undergone the common-envelope phase (e.g., Tylenda et al. 2011; Nandez et al. 2014; Chen & Ivanova 2024). While most LRNe are intrinsically faint ($M_V \gtrsim -6$ mag) events in the Milky Way, there is a growing sample of bright ($M_V \lesssim -12$ mag), extragalactic LRNe (Pastorello et al. 2021). ILRTs exhibit red continuua with Balmer emission lines and, in some cases, extremely long-lived outbursts (Smith et al. 2009). They remain enigmatic with evidence pointing to a variety of potential origins, including

electron-capture induced collapse from extreme asymptotic giant branch stars (e.g., Botticella et al. 2009) and outbursts from luminous blue variable-like stars (e.g., Jencson et al. 2019). The systematic identification of LRNe and ILRTs will provide insight into rare and understudied phases of stellar evolution.

LS4 may also discover an entirely new population of deeply enshrouded SNe, providing a more complete picture of massive star explosions. Many SNe, particularly those in dense, metal-rich star-forming regions, experience significant circumstellar dust reprocessing, leading to optical suppression (Bocchio et al. 2016; Serrano-Hernández et al. 2025). Finding these SNe is essential for constraining intrinsic transient rates, where it is known that many SNe are missed due to line-of-sight extinction (Kasliwal et al. 2017a; Jencson et al. 2019). This is especially pressing in galaxies with the highest star formation rates as their nuclear regions exhibit both the youngest stellar populations and largest line-of-sight extinction (e.g., Richmond et al. 1998). LS4 will be significantly more sensitive to these transients due to the sensitive and regular observations in the *i*- and *z*-bands.

6.7. Calcium-strong Transients

Relative to normal SNe, Calcium-strong (Ca-strong) transients are intrinsically faint and fast-evolving SNe with uncertain origins (e.g., Milisavljevic et al. 2017; Shen et al. 2019; De et al. 2020; Jacobson-Galán et al. 2020a). 56 The photospheric phase spectra of Ca-strong transients are dominated by helium features and resemble SNe Ib (Perets et al. 2010), while lacking the IGEs typically seen in thermonuclear SNe. Their spectra rapidly become optically thin, and their nebular phase spectra exhibit strong [Ca II] emission that dominates over relatively weak or non-existent [OI] (De et al. 2020). They are often found in remote environments, far from candidate elliptical/S0 host galaxies (Kasliwal et al. 2012; Yuan et al. 2013; Lunnan et al. 2017). Deep observational limits at the location of Ca-strong candidates show no signs of star formation or globular cluster hosts (Lyman et al. 2014; Lunnan et al. 2017). Thus, while they spectroscopically resemble SNe Ib with massive star progenitors, their preference for old stellar populations and remote environments favors a white dwarf progenitor (Shen et al. 2019).

The underlying explosion mechanism for these events is still hotly contested. On the massive star side, they could arise from the lower mass massive stars ($\sim 8-12\,M_\odot$) as an "electron-capture supernova" (Nomoto 1984; Kawabata et al. 2010), or ultra-stripped stars (Tauris et al. 2013, 2015; Moriya & Eldridge 2016). White dwarf origin channels have been suggested to include the merger of a C/O WD with a hybrid

⁵⁶ These events are also referred to as "Calcium-rich" transients in the literature (e.g., Kasliwal et al. 2012).

He/C/O WD (e.g., Jacobson-Galán et al. 2020a; Zenati et al. 2023), helium-shell detonations on low-mass CO WD (e.g., Waldman et al. 2011; Polin et al. 2019; Zenati et al. 2023), WD-NS mergers (Toonen et al. 2018; Zenati et al. 2019), and WD mergers with IMBHs (Sell et al. 2015). More speculative scenarios have been proposed to explain their large offset from galaxy centers involving a double WD system ejected from its host galaxy by interaction with a SMBH (Foley 2015), or single WD explosions, triggered by traversing asteroid-mass primordial BHs in dwarf satellite galaxies (Smirnov et al. 2024).

Early photometric observations of some objects have revealed double-peaked light curves, where the first peak is short-lived and associated with X-rays, likely indicating CSM interaction (e.g., Jacobson-Galán et al. 2020a, 2022b, but see also Bildsten et al. 2007 where decay of short-lived isotopes such as ⁴⁸Cr can result in early flux excess). The LS4 FOOT survey will capture early initial peaks and flux excesses from Ca-strong transients, while LSST will enable long-term monitoring as the flux rapidly fades. High-resolution images from LSST will place deep limits on the explosion environment of all LS4-discovered Ca-strong events.

6.8. 4MOST-TiDES Spectroscopic Follow-up

4MOST is a fiber-fed spectroscopic facility that packs \sim 2400 configurable science fibers into a 4.2 deg² FOV (de Jong et al. 2019). Over its 5 yr duration 4MOST TiDES (Frohmaier et al. 2025) will use 250,000 fiber-hours to obtain spectroscopic observations of transients and their host galaxies. The strategy for TiDES is simple, wherever 4MOST points within its \sim 18,000 deg² footprint, any live-and-bright ($r \leq 22.5$ mag) transients discovered by feeder surveys such as LS4 and LSST will have fibers placed on them. Every LS4-discovered transient will be brighter than the 4MOST observational limit (for a typical 2700 s exposure), meaning all LS4 SNe will be added into the TiDES observational queue.

To estimate the number of LS4 SNe that TiDES will observe, we used the input simulations from Frohmaier et al. (2025). We assumed every simulated SN within the LS4 footprint was detected if it was brighter than 21 mag. We then overlaid the 4MOST observing strategy from Frohmaier et al. (2025) to see which objects were observed as part of normal operations. We estimate that over a \sim 5 yr period TiDES will obtain spectra for around 5000 SNe in LS4. For transients that have faded below the TiDES limit prior to a spectrum being obtained, TiDES will request a spectrum of the host-galaxy. Additionally, 4MOST will host other surveys that enhance the LS4 science program with regular public data releases. The 4MOST Hemisphere Survey of the Nearby Universe (4HS; Taylor et al. 2023), will conduct a high-completeness census of galaxies in the local Universe (z < 0.15) and target around 6 million galaxies to z = 0.3 over $\sim 18,000 \, \text{deg}^2$. As a result, a

large proportion of LS4 discovered SNe will be hosted in galaxies observed by 4MOST.

6.9. Gravitationally Lensed Supernovae

gISNe are a new and novel probe of cosmology and highredshift astrophysics. The multiple images of glSNe produced by strong lensing permit a direct measurement of H_0 that is independent from the cosmic distance ladder, while magnification enables intrinsically fainter and more distant sources to be discoverable. Current estimates predict that H_0 can be measured to 1.5% with the first 3 yr of LSST WFD (Arendse et al. 2024). gISN discoveries to date have mostly been serendipitous from deep, high-resolution images (Kelly et al. 2015, 2022; Rodney et al. 2021; Chen et al. 2022; Frye et al. 2024; Pierel et al. 2024), with only three confirmed discoveries by wide-field surveys to-date (Quimby et al. 2013; Goobar et al. 2017, 2023). In the next decade, the unprecedented volume probed by LSST will enable the first statistical sample of glSNe, with estimates reaching up to $\sim 100 \, \mathrm{yr}^{-1}$ (Oguri & Marshall 2010; Goldstein et al. 2019; Sainz de Murieta et al. 2023; Arendse et al. 2024). LS4 will support the discovery and science possible with glSNe.

Wide-field surveys that monitor known lensed galaxies can efficiently discover gISNe. This can be achieved with a "watchlist" of known lenses, and can also include candidate lenses, which typically consist of luminous red galaxies (LRGs) and galaxy groups and clusters, which collectively make up a large proportion of the total strong lensing cross-section in the Universe (e.g., Robertson et al. 2020). Discoveries by observations of resolved multiple images will also be possible for gISNe in the upper tails of the image separation distribution: \sim 5% will have image separations larger than the LS4 pixel scale (1"pixel⁻¹), which can be resolved either directly or via PSF deconvolution (Sainz de Murieta et al. 2023; Millon et al. 2024). Image separation and magnification are approximately independent: most of the gLSNe discoveries should come from magnified but unresolved systems in known lenses (Sainz de Murieta et al. 2024), however this relies on us having a large sample of known lenses.

Due to their standardizable nature, glSNe Ia can be identified when a SN Ia is far too luminous for the redshift of its "host," which in the case of a glSN found in ground-based imaging is the lens galaxy rather than the true SN host galaxy (e.g., Goobar et al. 2017, 2023). Spectroscopic observations were essential to identify the glSNe found by ground-based surveys, but most glSN candidates will be faint and not receive a spectrum. With a higher cadence than LSST WFD, LS4 light curves will enable the photometric classification of SNe Ia. Furthermore, the red-sensitivity of LS4 will help to identify glSNe which will occur at substantially higher redshifts than the "normal" unlensed LS4 SN Ia population.

Assuming an *i*-band detection limit of $m_i = 20.5$ mag, a \sim half-sky survey should discover \simeq 0.2 glSNe yr⁻¹ (Sainz de Murieta et al. 2023). While this estimate is somewhat small, the true number of known glSNe observed with LS4 will be larger than this in reality, since LSST-discovered systems will permit sub-threshold measurements of glSNe within LS4. Finally, to increase the discovery rate of glSNe we will perform offline stacking of LS4 LEG and FOOT images to search for slow-evolving SNe below the LS4 detection threshold with red colors ($g-r\gtrsim 0.75$ mag). While these candidates will be faint, they will still be brighter than the detection limit of 4MOST/TiDES and SoXS, which will enable follow-up of these highly valuable targets.

7. Multi-messenger Astrophysics

7.1. Electromagnetic (EM) Follow-up of Gravitational Wave Sources and Poorly Localized GRBs with LS4 and LSST

The discovery of the an EM counterpart to the binary NS merger, GW 170817, launched the era of GW+EM multimessenger astrophysics (Abbott et al. 2017a; Margutti & Chornock 2021). While the direct detection of GWs from astrophysical sources has enabled an exciting new view of the cosmos, GW signals paired with EM observations provide an unprecedented probe of astrophysics. The first EM signal from GW 170817 was a short-duration GRB (SGRB), GRB 170817A, which provided direct evidence that at least some SGRBs come from NS-NS mergers (Abbott et al. 2017b). As observations across the EM spectrum of GW 170817 demonstrated, the identification of an EM counterpart provides immense scientific benefits, including: improved localization leading to a solid hostgalaxy identification; determination of the source distance and energy; characterization of the progenitor's local environment; the ability to break model degeneracies between distance and inclination of the binary system; and insight into the hydrodynamics of the merger. Furthermore, identification of the EM counterpart facilitates other fields of study such as determining the primary sites of heavy r-process element production, placing limits on the NS equation of state, making independent measurements of the local Hubble constant, H_0 , and further elucidating their connection to SGRBs (Abbott et al. 2017a, 2017c; Hjorth et al. 2017). See Margutti & Chornock (2021) for a review of the EM+GW properties of GW 170817 and the immense scientific impact of that discovery.

Exploiting the success of multi-messenger astronomy in the next decade will require the continued investment in observational resources. The fourth observing run (O4) of the LVK collaboration is currently planned (at the time of this writing) to end on 2025 November 18.⁵⁷ Upon completion of

instrumental upgrades, LIGO, Virgo and KAGRA are expected to re-start operations with a fifth observing run (O5) in 2027 with improved sensitivity and localizations⁵⁸ resulting in improved capabilities for counterpart discovery (Kiendrebeogo et al. 2023; Shah et al. 2024). With its 5 yr duration, LS4 will overlap with the tail end of O4 and all of O5. Furthermore, LSST also begins in the second half of 2025 and up to 4% of the LSST observing time has been approved for ToO programs (see Andreoni et al. 2024 and references therein). LS4, in concert with LSST ToO observations, will provide an agile, wide FOV system that is well suited for GW follow-up. Synergy between LS4 and LSST operations will maximize the scientific potential and discovery power of both surveys. For example, the best use of the large aperture of LSST is to follow up the most distant mergers (Margutti et al. 2018; Andreoni et al. 2022b), which will have the faintest EM counterparts that are simply out of reach for any other observing facility (Figure 6). Together, LSST and LS4 can be the premiere discovery engine of EM counterparts to GW sources in the Southern Hemisphere.

Meanwhile, the Fermi satellite (Meegan et al. 2009) is the most prolific workhorse for GRB discovery finding \sim 240 yr⁻¹ (Bhat et al. 2016). Given that the typical GRB localizations are \sim 50–100 deg² (Connaughton et al. 2016), few facilities attempt to find Fermi GRB afterglows. Fermi-discovered SGRBs, especially those with characteristics similar to GRB 170817A, are especially interesting because they may be hiding in the nearby universe (von Kienlin et al. 2019). SGRBs provide a beacon for finding NS mergers in the local Universe (and when GW interferometers are offline this represents the most reliable path to discovery).

LS4 will conduct ToO observations of the best-localized GW events and SGRBs in the local Universe ($d \lesssim 200 \, \text{Mpc}$), with these primary scientific goals:

- (i) Growing the sample of EM counterparts to GW events to conduct statistically rigorous systematic studies to understand the diversity of EM emission, their host environments, the nature of merger remnants, and their contribution to the chemical enrichment of the universe through *r*-process production, which shapes the lightcurves and colors of the "kilonovae" (KNe) associated with GW events (e.g., Metzger et al. 2015).
- (ii) Sampling the very early KN emission (e.g., ≤10 hr postmerger) to identify emission mechanisms beyond the KN (e.g., neutron precursor, shock-cooling, e.g., Piro & Kollmeier 2018). Despite the fact that the optical counterpart of GW 170817 was discovered less than 11 hr post-merger (e.g., Arcavi et al. 2017b; Coulter et al. 2017; Cowperthwaite et al. 2017; Drout et al. 2017;

⁵⁷ See https://observing.docs.ligo.org/plan/ for the most up to date information on O4.

⁵⁸ https://www.ligo.caltech.edu/page/observing-plans

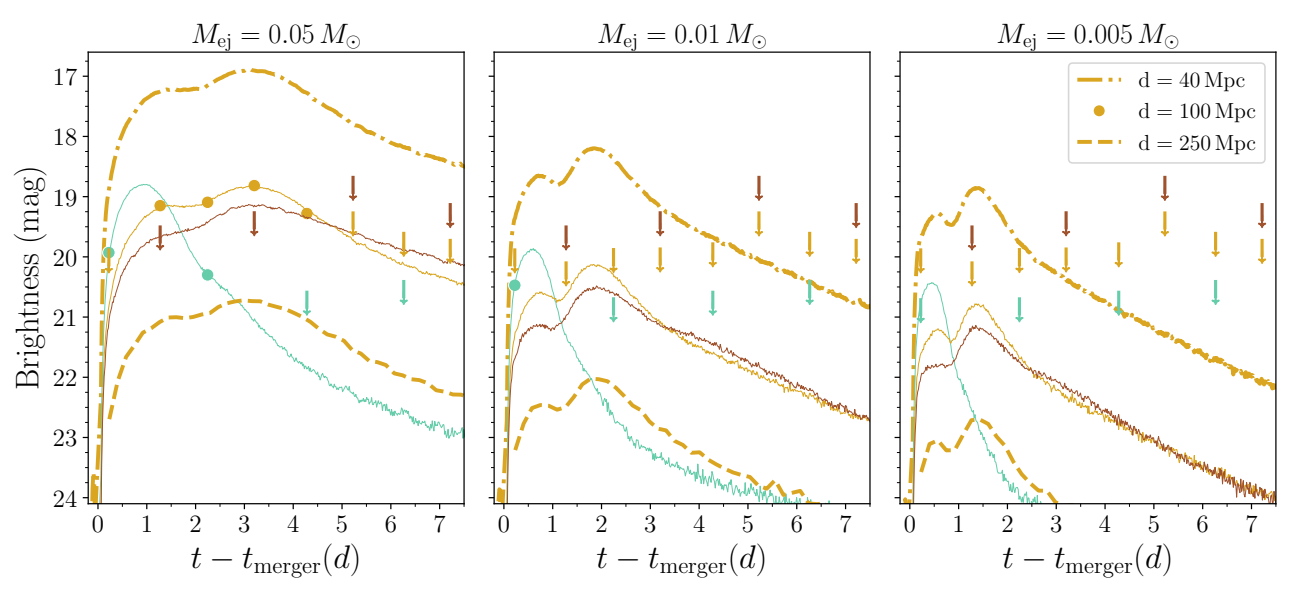


Figure 6. Simulated LS4 light curves for a kilonova (KN) with ejecta velocity $v_{\rm ej} = 0.15c$ and different ejecta masses, $M_{\rm ej} = 0.05$, 0.01, $0.005~M_{\odot}$, shown in the left, middle, and right panels, respectively, each at three representative distances of 40, 100 and 250 Mpc. The KN luminosity is not a strong function of $v_{\rm ej}$ and values within 0.1–0.2c give comparable results. The $0.05~M_{\odot}$ model is closest to the observed KN properties of GW 170817. The LS4 g, i, and z light curves for observations starting \sim 6 hr after the NS–NS merger are shown for the 100 Mpc model, while only the simulated i-band evolution is shown for the 40 and 250 Mpc models (thin lines show the simulated g, i, and z evolution at 100 Mpc). The panels extend to $i \approx 24.5$ mag, which is the typical detection limit for LSST in a 30 s exposure (Jones 2022). When the ejecta mass is large, LS4 can detect a KN to distances \gtrsim 100 Mpc. For much lower masses, LS4 will only detect KNe to a few 10s of Mpc. Symbols the same as Figure 3.

Kasliwal et al. 2017b; Lipunov et al. 2017; Smartt et al. 2017; Soares-Santos et al. 2017; Tanvir et al. 2017; Valenti et al. 2017; Villar et al. 2017), these observations were still unable to definitively determine the nature of the early time emission.

- (iii) Finding the first EM counterpart of a merger of a NS-BH. This system might produce a KN, but the ejecta mass depends on the mass ratio of the binary and the NS equation of state, and in some cases there may be no material ejected at all (e.g., Foucart et al. 2018). It is also unclear if NS-BH mergers will be able to produce the bright early-time blue emission seen in GW 170817 (Metzger et al. 2015).
- (iv) Exploring the unknown of EM counterparts to BH-BH mergers (Graham et al. 2020) and to unidentified GW sources. Utilizing the LS4 public alerts that fall within the LVK sky maps region we will search for BH-BH GW events.
- (v) Measuring H_0 to 2%–8% precision (Palmese et al. 2019) using the standard siren method (Schutz 1986) for the GW events with an identified counterpart. These constraints can further be improved with well-sampled KN light-curve observations (Dhawan et al. 2020). A precise and accurate measurement of H_0 from standard sirens could help clarify whether the observed H_0 tension between late (Riess et al. 2019) and early (Planck Collaboration et al. 2020) time Universe measurements

- arises from beyond- Λ CDM physics or unknown systematics (e.g., Verde et al. 2019).
- (vi) Pinpointing the origins of nearby SGRBs, independent of their GW signals, by identifying and localizing their counterparts.
- (vii) Testing the gravitational lensing interpretation of bright GW sources detected in LVK in the putative gap between the heaviest NS and the smallest stellar remnant BHs (Smith et al. 2023; Andreoni et al. 2024). There are many uncertainties associated with the predicted rate of gravitationally lensed BNS mergers, but it is predicted that LVK O5 will discover no more than 1 yr⁻¹ (e.g., Magare et al. 2023; Smith et al. 2023) with a corresponding false positive rate of $\sim 1 \text{ yr}^{-1}$ (Andreoni et al. 2024). While such events will be rare they provide an opportunity to unlock unique scientific opportunities including the first glimpse of the GW source population at redshifts of $z \simeq 1-2$ (Figure 7), unprecedented tests of General Relativity (GR) enabled by a step change in the precision of GW polarization measurements (e.g., Goyal et al. 2021), and a new ultra-precise probe of the Hubble tension (e.g., Birrer et al. 2025). Among the most exciting prospects is the very early detection of the lensed KN counterpart to the lensed GW when its second image arrives at Earth with potential to be the earliest possible detection of a KN counterpart, and thus yield unprecedented constraints on the underlying physics (Nicholl & Andreoni 2025).

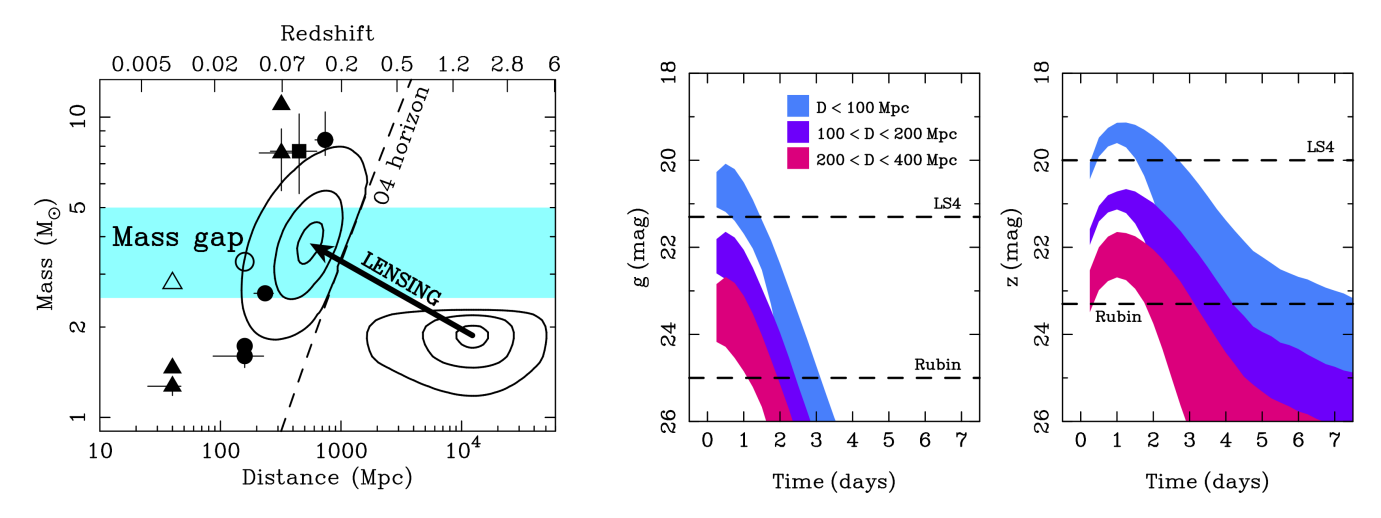


Figure 7. Left: mass–distance plane for binary compact object mergers detected by LVK, showing how lensing makes distant binary NS mergers appear as being more massive and closer than they really are. We expect most of the lensed BNS mergers will be inferred by the LVK in low latency to be located in the mass gap between the heaviest NS and the lightest BHs. Contours show the 90th, 50th, and 10th percentile of the predicted lensed population as inferred by LVK assuming no lensing ($\mu = 1$) bright-ward of the horizon, and the true distribution faint-ward of the horizon (dashed line). Filled symbols are the masses of individual compact objects and open symbols are the merger remnant. Squares, triangles and circles show detections from LVK runs O1, O2, and O3, respectively. Center and Right: predicted g- and z-band light curves of lensed KN counterparts to lensed binary NS mergers, as a function of the distance to them that LVK infer in low latency assuming $\mu = 1$. LS4 target of of opportunity observations of regular depth will have the sensitivity to detect the brightest (apparently loudest and nearest) lensed events (upper dashed line), with strong potential to reach fainter systems by integrating for longer on the best localized events, following the approach outlined by Andreoni et al. (2024). The relative sensitivity of LS4 and Rubin is indicated by the difference between upper and lower dashed lines. The width of the light curve bands show the central 90% of the predicted probability density for the lensed population.

7.2. Follow-up of Neutrino Sources

LS4 will search for EM counterparts of neutrino sources. For decades, there were only two examples of source-specific multi-messenger detections, both in MeV neutrinos: from the solar interior (starting in the 1960s), and from the nearby CCSN 1987A (Hirata et al. 1987). The era of high-energy neutrino astronomy started with the discovery of an astrophysical diffuse flux of TeV-PeV neutrinos (IceCube Collaboration 2013). Roughly 10% of that flux could be attributed to the Galactic plane (The Icecube Collaboration et al. 2023). The origin of the remaining, extragalactic flux is still an open question. Identified candidate neutrino sources include the close-by Seyfert galaxy NGC 1068 (The IceCube Collaboration et al. 2022) and the flaring gamma-ray blazar TXS 0506 +056 (IceCube Collaboration et al. 2018b), but these individual sources can contribute at most a few percent to the diffuse flux. Furthermore, several extreme accretion flares (e.g., AT 2019dsg, AT 2019fdr and AT 2019aalc; Stein et al. 2021; Reusch et al. 2022; Veres et al. 2024) have been found in spatial and temporal coincidence with high-energy neutrino events. These accretion flares might be TDEs. While the neutrino emission from Seyfert galaxies is expected to be steady over time, the emission from blazars and accretion flares is expected to be variable or transient and is accompanied by a variable or transient EM counterpart that could be detected with LS4. Other neutrino source candidates

with distinct EM counterparts include interacting SNe (e.g., Murase et al. 2011, 2019; Margutti et al. 2014; Zirakashvili & Ptuskin 2016; Petropoulou et al. 2017; Murase 2018; Wang et al. 2019; Fang et al. 2020; Sarmah et al. 2022; Waxman et al. 2025), choked-jet SNe (e.g., Mészáros & Waxman 2001; Razzaque et al. 2005; Horiuchi & Ando 2008; Murase & Ioka 2013; Nakar 2015; Senno et al. 2016), and GRBs (see Kimura 2023, and references therein).

The challenge when using neutrinos as triggers for EM follow-up observations is to suppress the large atmospheric background that is present in water and ice Cherenkov detectors such as IceCube (Aartsen et al. 2017a) and KM3NeT (Adrian-Martinez et al. 2016). IceCube publically releases a stream of single high-energy events (typically around 100 TeV) with a high probability (≥30%) to be of cosmic origin (Aartsen et al. 2017b). A recent update to this stream⁵⁹ reduced the median 90% angular uncertainty to 1.26 deg. Alternatively, spatial and temporal clusters of lower-energy neutrinos (1–10 TeV) can be used to suppress the atmospheric background, which is mostly isotropically distributed in the sky. Short clusters (100–1000 s) are selected to target short transients such as GRBs or choked-jet SNe (Aartsen et al. 2019), while longer time windows are used to

⁵⁹ https://roc.icecube.wisc.edu/public/docs/IceCube_Update_Muon_Alert_ Reco.pdf

search for TDEs, AGN flares or interacting SNe (The IceCube Collaboration et al. 2016; Abbasi et al. 2025).

Current rates of neutrino alerts from IceCube are roughly $30\,\mathrm{yr}^{-1}$ for single high-energy events. Multiplets with maximal duration of $1000\,\mathrm{s}$, $30\,\mathrm{days}$ and $180\,\mathrm{days}$ will be released with an expected rate of a \sim few per year in the near future. Furthermore, detectors under construction are expected to contribute a realtime neutrino stream of $\mathcal{O}(10\,\mathrm{yr}^{-1})$ during the run time of LS4. The scientific potential of partial detectors was illustrated by the detection of a 200 PeV neutrino event by KM3NeT-ARCA with only $\sim \! 10\%$ of the detector deployed (KM3NeT Collaboration et al. 2025).

Ongoing observations and improvements in TeV-PeV neutrino observatories are likely to yield a large sample of astrophysical neutrinos, potentially enabling the detection of EM counterparts on a regular basis. IceCube is currently in operation, while Baikal-GVD and KM3NeT-ARCA are operating with partial detectors until they complete their arrays in the late 2020s. New neutrino telescopes are planned, which will expand the sky coverage, sensitivity, and energy range compared to current instruments. It is now imperative to expand the sample of neutrino sources with EM counterparts to confirm their physical associations with high statistical confidence, advance our understanding of these sources, and the physics of the neutrino emission.

7.3. Comparison to Existing/Planned Facilities in the Southern Hemisphere

8. Cosmology

SNe Ia have famously been used as cosmological distance indicators, and they played an essential role in the discovery of the accelerating expansion of our Universe (Riess et al. 1998; Perlmutter et al. 1999). SNe Ia remain a key cosmological probe, especially for measuring the recent expansion history of the Universe ($z \lesssim 1$), where dark energy drives the accelerating expansion (for a review, see Goobar & Leibundgut 2011). Consequently, SN Ia data continue to provide strong constraints on dark energy (Betoule et al. 2014; Scolnic et al. 2018; Brout et al. 2022; Rubin et al. 2025; DES Collaboration et al. 2024). In particular, current measurements aim to resolve

the question of whether the dark energy density is constant (i.e., like Λ), or a dynamical phenomenon involving new fields or modifications of the law of gravity beyond GR.

Recent results driven by SN Ia data (Rubin et al. 2025; DES Collaboration et al. 2024) combined with Cosmic Microwave Background (CMB; Planck Collaboration et al. 2020) and Baryon Acoustic Oscillation (BAO) constraints, show a 2.5σ – 3.9σ discrepancy with Λ (e.g., Adame et al. 2025). The dark energy equation of state can be parameterized as w(a) = $w_0 + w_a(1-a)$ (where a = 1/(1+z) is the scale factor of the cosmic expansion), and these new measurements prefer models where $w_0 > -1$ and $w_a < 0$, implying that the dark energy density is dynamical, i.e., evolving with time. Adding to the challenge, there is a so-called "Hubble tension" where the local distance ladder measurements of H_0 based on using standardized stars (e.g., Cepheids, Tip of the Red Giant Branch, J-region Asymptotic Giant Branch) to calibrate distances to SN Ia host galaxies is 2%-8% larger than what is inferred from early Universe CMB observations, using Λ plus cold dark matter (ACDM) and BAO measurements to extrapolate to the present time (Planck Collaboration et al. 2020; Riess et al. 2022; Freedman & Madore 2023; Freedman et al. 2025). This discrepancy has stubbornly resisted resolution. Dynamical dark energy or a break-down in the GR theory used for cosmological inference would point to new fundamental physics. Overall, deviations from the expectations of the ACDM model are strongest at low redshifts, making nearby SN Ia data sets such as that planned for the LS4 survey critical for fundamental physics.

8.1. Anchoring the SN Hubble Diagram

Continued study of this acceleration and the nature of dark energy will be conducted with large samples of SNe at high redshift by both LSST (pushing to $z \sim 1$) and Roman (pushing to $z \sim 2$). To effectively measure cosmological parameters, these high-z samples need to be anchored with hundreds or thousands of well-calibrated SNe Ia at low redshift. Recent efforts compiling such samples (e.g., Rubin et al. 2025; Rigault et al. 2025) are largely concentrated in the northern hemisphere and do not (yet) have the calibration precision that we plan to attain with LS4. A Hubble diagram composed of low-to-high redshift SNe discovered and observed by overlapping shallower and deeper surveys can be placed on a uniform magnitude system, mitigating a limiting source of uncertainty in current data. Even so, the relative motion of the local volume induced by large scale structure can imprint an offset on local SN brightnesses relative to those covering large volumes where this effect is averaged-out (Hui & Greene 2006). An equally large ($N \approx 4000$) sample in the southern hemisphere will help to average-out this offset, which is one of the primary cosmology goals of LS4.

8.2. Peculiar Velocities

The combination of SNe from the northern and southern hemispheres will also improve our ability to measure the power spectrum of galaxy/dark matter motions across the entire sky, which will, in turn, better constrain measurements of the growth of structure. The scatter along the redshift axis of the SN Hubble diagram induced by peculiar velocities is especially pronounced at lower redshifts. Spatial correlations in the velocity scatter are seeded by the same dark matter field that gives rise to galaxy-count over-densities. The peculiar velocity power spectrum is related to the dark matter power spectrum by a proportionality factor $P_{\nu\nu} \propto (fD)^2$, where D is the spatially independent "growth factor" in the linear evolution of density perturbations and $f \equiv \frac{d \ln D}{d \ln a}$ is the linear growth rate where a is the scale factor (Hui & Greene 2006; Davis et al. 2011). When considering the local Universe it is common to express the growth factor as a constant normalized by a fiducial value, $D = \sigma_8/\sigma_{8,\text{fid}}$. More generally, GR, f(R)gravity (e.g., Buchdahl 1970), and Dvali-Gabadadze-Porrati gravity (Dvali et al. 2000) follow the relation $f \approx \Omega_M^{\gamma}$ with $\gamma = 0.55, 0.42, \text{ and } 0.68, \text{ respectively (Linder & Cahn 2007)}.$ Using this parameterization to model gravity, peculiar velocity surveys probe γ through fD, whose γ -dependence is plotted in Figure 2 of Linder (2013). SNe Ia with z < 0.1 to first order measure the strength of gravity and with redshift-dependence can distinguish between GR and competing theories of modified gravity.

Over its full duration, LS4 will discover and measure light curves of \sim 4000 SNe Ia out to $z\approx$ 0.1. The relatively sparse cadence and large aperture for LSST WFD are not well suited for precision light curves of low-z SNe, as shown in Figure 3. LS4 will do considerable work to fill in the gaps in low-z LSST observations with both the LEG and FOOT surveys, which will enable (i) robust identifications of SN Ia candidates well before peak in order to obtain maximum-light spectra, and (ii) easy photometric classifications via the i- and z-band secondary maxima, prominent in normal SNe Ia, for those without spectra. Thus, LS4 SNe Ia will tightly constrain the growth of structure in the low-redshift Universe.

Projections using the FLIP code of Ravoux et al. (2025) indicate that 4000 SNe Ia to $z\approx 0.1$ over the LS4 footprint can produce 13/15/22% uncertainties in $f\sigma_8$ from peculiar velocities alone and 9/11/15% uncertainties when combined with the galaxy density field from redshift surveys, respectively for 0.08/0.11/0.15 mag standardization dispersion. The dispersion realized for LS4 will depend in part on the extent and quality of spectroscopic follow-up we are able to obtain, or the standardization improvements our redder bandpasses may offer. Studies indicate that the photometric misclassification of SNe Ia with LSST-quality light curves will induce a bias in $f\sigma_8$ measurements that is less than the statistical error for z<0.16 for the case of 0.15 mag standardization dispersion (Rosselli

et al. 2025). Thus, we can expect that a survey relying solely on joint LS4+LSST discoveries and photometry coupled with spectroscopic host-galaxy redshifts would be competitive, but also has the potential to be improved substantially. Our forecast values are comparable to the 15.3/6.5% velocity-only and velocity+galaxy results anticipated for DESI (Saulder et al. 2023; Said et al. 2025) and the 5% velocity+galaxy forecasts for 4MOST (Taylor et al. 2023), calculated using (somewhat more optimistic) Fisher matrix forecasts for the Fundamental Plane and Tully–Fisher galaxy-based distance indicators.

We note that these efforts are complementary to the ongoing ZTF survey, since ZTF and LS4 are in different hemispheres covering different parts of the sky. Combining SNe from the two surveys roughly doubles the survey volume and increases by 4 the number of SN pairs, tightening the $f\sigma_8$ uncertainty by a factor $\sqrt{2}$.

LS4 will provide a low-redshift anchor on $f\sigma_8$ at 0 < z < 0.1 whereas precise measurements at higher redshifts will come from redshift space distortions derived from galaxy surveys (Howlett et al. 2017). When both probes are combined, the redshift-dependent evolution of $f\sigma_8$ will provide a strong test of GR and other gravitational models (Kim & Linder 2020).

8.3. Reducing the Uncertainty on SNIa Distance Measurements

Nearby SNe Ia are bright enough that their diversity can be studied in detail, enabling the investigation of potential astrophysical biases that could affect the inference of cosmological parameters. For such nearby SNe Ia, LS4 will provide z-band light curve observations that are currently rare, and more i-band observations (relative to ZTF). These data can help solve the complex origin of SN-host correlations by providing a longer wavelength baseline, e.g., for studying the effects of host-galaxy dust, while also improving photometric classification by exploiting the i- and z-band secondary maxima seen in SN Ia light curves (e.g., Riess et al. 1996; Kasen 2006). Furthermore, the overlap in time and sky coverage with LSST enables extended phase coverage (see e.g., Figure 3). These synergistic observations will provide an unprecedented opportunity to study complex nonlinear and color-dependent standardization effects.

SN Ia are empirically calibrated distance indicators because their progenitors and explosion mechanism are insufficiently known, and predictive models at the required few-mmag level do not yet exist. Light-curve standardization reduces the natural dispersion of \sim 0.4 mag to 0.12–0.15 mag (Phillips 1993; Riess et al. 1996; Tripp 1998). Spectroscopic standardization (Boone et al. 2021; Stein et al. 2022) and some NIR data (Barone-Nugent et al. 2012) can reduce this scatter to \sim 0.08 mag. The remaining scatter is unexplained by measurement or modeling uncertainties, leaving ample room for

unaccounted effects that could bias the inferred distances. Thus, the uniformity and differences in the observed calibration parameters of SNe Ia as a function of redshift and host environment are an area of active investigation in order to ensure they are sufficiently reliable standardizable candles for measuring dark energy and H_0 .

Within this context, large samples have clearly demonstrated that the SN Ia standardized brightness correlates with host properties. For example, SNe Ia in massive galaxies are ~ 0.1 mag brighter than those in low-mass galaxies (Kelly et al. 2010; Sullivan et al. 2010; Childress et al. 2013; Rigault et al. 2013). Further investigation of this correlation has suggested it could originate from a progenitor effect, such that SN Ia associated with young stellar environments are intrinsically fainter (Rigault et al. 2013, 2020), or variations in host galaxy dust properties along the SN Ia line of sight (Brout & Scolnic 2021; Johansson et al. 2021), or both. The offset in magnitude between SNe Ia in low and high-mass hosts (often referred to as the "mass-step") has been used as a third standardization parameter in recent cosmological analyses (e.g., Betoule et al. 2014; Scolnic et al. 2018; Riess et al. 2022; Rubin et al. 2025; DES Collaboration et al. 2024). This correction is applied despite the "mass-step" likely being a proxy for a more fundamental effect driving the magnitude offset. Spectroscopic standardization reduces such "steps" by roughly a factor of 2-3 (Boone et al. 2021), indicating that much of the effect arises from the limitations of the presentday light-curve standardization method itself, and further indicating that SNe Ia do in fact transmit the information necessary to improve their standardization.

Such studies, with the most recent examples from the large ZTF DR2 data set include: confirming that the stretch parameter commonly used to account for the luminosity-decline rate relation (Phillips 1993; Perlmutter et al. 1997) is nonlinear (Amanullah et al. 2010; Rubin et al. 2015; Garnavich et al. 2023; Larison et al. 2024; Ginolin et al. 2025); clearer evidence of the expected intrinsic SNe Ia color component in addition to reddening by dust (Mandel et al. 2017, 2022; Rubin et al. 2025; Ginolin et al. 2025); even larger "steps" than the canonical "mass-step" using different indicators and/or unbiased samples (Rigault et al. 2020; Ginolin et al. 2025). Even for the host-galaxy dust component, cosmology applications must consider R_V variations (Amanullah et al. 2015; Huang et al. 2017; Mandel et al. 2017, 2022; Brout & Scolnic 2021; Rubin et al. 2025; Grayling et al. 2024; Ginolin et al. 2025).

Finally, we note that other contemporaneous surveys will enrich the LS4 SN cosmology data set. LSST over the full LS4 footprint, and Euclid and Roman over some of the footprint, will provide exquisite, deep, higher resolution imaging, in more bands, of the LS4 host galaxies. 4MOST and DESI will provide high-quality spectra of many of these same host galaxies. Combined, these offer a significant advantage over

many previous studies of SNIa standardization residuals correlated with global and local host galaxy properties.

8.4. Cosmology with SNe II-P

SNe II as cosmological probes have lagged behind their brighter and better calibrated cousins, SNe Ia, but they nevertheless hold cosmological value. Recent studies have used new samples of SNe II and demonstrated that the subset with long photometric plateaus, SNe II-P, have outstanding cosmological utility (for a review, see Nugent & Hamuy 2017).

There are multiple advantages for using SNe II to probe cosmology over SNe Ia: (i) the progenitor systems of SNe II-P are well understood; (ii) SNe II-P are more numerous per unit volume by a factor of 3; and (iii) the plateau phase lasts for \sim 100 days, allowing ample time to take a spectrum of the event and measure its expansion velocity. Recently, the socalled Standard Candle Method (SCM. Hamuy & Pinto 2002; Nugent et al. 2006; Olivares et al. 2010) achieved $\sigma_M = 0.27 \, \text{mag}$ with nearly 90 nearby SNe II-P (de Jaeger et al. 2020). Given the advantage in number density, the relative weight of SNe II-P is comparable to SNe Ia for the peculiar velocity measurements ($\sigma_M = 0.12-0.15 \text{ mag}$). Measuring distances with SNe IIP requires a precise measurement of the explosion date. In the traditional expanding photosphere method (e.g., Leonard et al. 2002), one can overcome this hurdle by taking multiple spectra (Kirshner & Kwan 1974) and simultaneously solving for the luminosity and explosion date. However, the LS4 FOOT cadence will constrain explosion dates to within a day, obviating the need for multiple spectra and allowing facilities like DESI (DESI Collaboration et al. 2016) and 4MOST/TiDES to leisurely take a single spectrum during the plateau phase. When coupled with the exquisite multi-color photometry from LS4, distance measurements out to z = 0.05 will be straightforward, not only improving peculiar velocity measurements, but also contributing to an independent measurement of H_0 (de Jaeger et al. 2022; see de Jaeger & Galbany 2024 for a review).

8.5. Precise Instrumental Throughput Calibration

The precise determination of luminosity distances to objects at different redshifts requires knowing the instrumental response function of the astronomical instrument, and making correspondingly precise corrections for extinction along the line of sight to the source. Reaping the benefit of improved statistics from large increases in the number of detected SNe requires lowering the floor on systematic errors due to photometric calibration (Stubbs & Brown 2015).

The sensitivity function $S(\lambda)$ of a telescope+camera system establishes both the zero-points and the bandpass shapes. Zero-points are typically determined using standard stars, such as the CALSPEC suite of spectrophotometric standards (Bohlin et al. 2020), and the more recently established network of

fainter white dwarf standards (Boyd et al. 2025). However, these do not provide the bandpass shapes with sufficient fidelity for cosmology with SNe. Moreover, cosmology with SNe relies on relative distances—so it is the filter-to-filter zero-points that need to be determined at the few-mmag level.

A method to determine both the relative filter zero-points and the bandpass shapes exploits the fact that the quantum efficiency of silicon photodiodes can be determined at the part-per-thousand level. Using this as the metrology basis for photometry requires transferring that calibration knowledge onto the astronomical imaging system (Stubbs & Tonry 2006). This has now been shown at the few-mmag level (Souverin et al. 2025).

The LS4 survey will utilize both celestial and terrestrial calibrators to establish the relative zero-points across the *giz* passbands. We will deploy PANDORA, a device that injects a known dose of monochromatic photons into the telescope pupil, to measure the instrumental response function (Sjoberg et al. 2025). This knowledge will be supplemented with a comparison of synthetic and on-sky photometry of white dwarf calibration objects, and all-sky cross-calibration with the Rubin photometric system. On occasion there will be LS4 SN observations simultaneous with LSST, greatly strengthening the calibration between the SN samples from these two surveys.

9. Stellar Lensing, Flares and Variability

For decades several surveys have regularly monitored select fields in the Milky Way Galactic bulge and in the Magellanic Clouds with a comparable depth and cadence to what is planned for LS4, including: OGLE (Udalski et al. 1992), the Massive Compact Halo Objects (MACHO) project (Alcock et al. 1996), EROS (Ansari et al. 1996), the Korea Microlensing Telescope Network(KMTNet; Kim et al. 2018), the Microlensing Observations in Astrophysics survey (MOA; Sumi et al. 2003). The entire southern sky has also been observed repeatedly by surveys such as Gaia, the Transiting Exoplanet Survey Satellite (TESS), ASAS-SN, and ATLAS. The cadence from Gaia is sparse compared to LS4 and the bandpasses are fewer and non-standard. Surveys such as ASAS-SN and TESS observe with higher cadence, but, critically, the LS4 survey will reach single-epoch depths \sim 5 mag deeper than these precursors. As such, the same Galactic variables found in ASAS-SN or TESS could be observed at ten times the distance within a thousand times larger volume. In its first three years of operation ZTF found $\mathcal{O}(10^6)$ variables (Ofek et al. 2020), and we expect to find and characterize a similar number with LS4.

9.1. Microlensing

Gravitational microlensing occurs when a massive "lens" object passes near the line of sight between a luminous "source" object and an observer and the lens bends the light

path from the source. This produces a transient brightening (photometric microlensing) and apparent positional shift (astrometric microlensing) of the source star. Characterizing these events enables direct measurement of the mass of the lens. Thus, microlensing is an ideal method for detecting compact objects, dim stars, brown dwarfs, and cool planets. Within the LS4 SOLE survey of the Galactic plane and bulge, photometric microlensing events will be discovered. Particularly interesting events (e.g., BH candidates) may be followed up with high-resolution imaging from space or with ground-based adaptive optics to measure the astrometric signal during the event, or as late-time follow-up to observe the lens-source separation (e.g., Lu et al. 2016; Abdurrahman et al. 2021).

In gravitational lensing events, the source's light is bent around the lens' Einstein ring, and parameterized by the angular size $\theta_{\rm E}$, the Einstein ring radius crossing time $t_{\rm E}$, and the microlensing parallax $\pi_{\rm E}$. Observation of photometric microlensing measures $t_{\rm E}$ and $\pi_{\rm E}$, but additional information is typically required to break the mass–distance degeneracy and fully characterize the lens system. For the study of stellar mass black holes, we can use follow-up astrometry to measure $\theta_{\rm E}$ and determine the lens mass. One isolated black hole has been detected with this technique so far (OGLE-2011-BLG-0462, Sahu et al. 2022; Lam & Lu 2023), and LS4 will help identify new candidates to build a sample of several black holes.

While LSST will be capable of finding microlensing events, the WFD cadence is not ideal for characterizing average microlensing events (see Abrams et al. 2025a). A ~1 day cadence is critical to fully measure the shape of the microlensing light curve and the microlensing parallax (see, e.g., Lam 2023). For events detected in both surveys, LSST will provide photometry with higher precision and additional filters, improving the output of multi-band event fitting.

9.1.1. In the Galactic Plane

The characteristics of microlensing events are determined by the spatial and kinematic distributions of luminous objects and massive objects in the Milky Way, which probes the structure of the Galaxy. To date, the majority of ongoing microlensing surveys have primarily been focused on the Galactic bulge and the areas around it. The LS4 SOLE survey offers a valuable opportunity to search for microlensing throughout the plane from a southern observing site. Furthermore, *z*-band observations will allow LS4 to peer deeper into the most extinguished regions in the Galactic plane than surveys that only extend redward to the *r* and/or *i* bands (see Figure 8). LS4's multi-filter configuration will provide useful color information since microlensing events are achromatic to first order, unlike many other forms of variability.

Several studies have analyzed microlensing events detected in ZTF observations in and out of the Galactic plane (e.g., Mróz et al. 2020; Rodriguez et al. 2022; Medford et al. 2023;

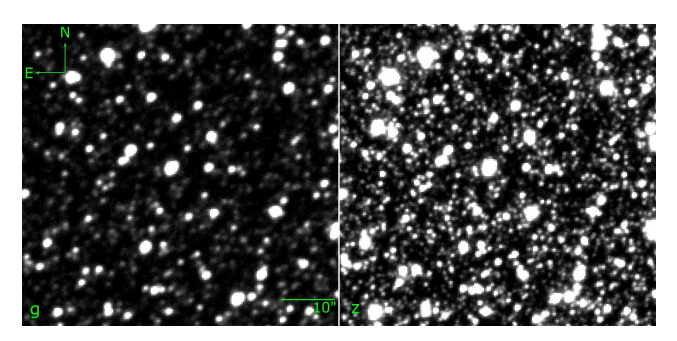


Figure 8. Comparison of the number of stars that can be observed in blue vs. red filters for a high-extinction field toward the Galactic plane. Images are $60^{''} \times 60^{''}$ cutouts from a DECaPS-East deep drilling field (Graham et al. 2023) located at right ascension and declination $\alpha_{\rm J2000}=07^{\rm h}~45^{\prime}~16^{\prime\prime}/8$, $\delta_{\rm J2000}=-26^{\circ}~15^{\prime}~00^{\prime\prime}/0$. North is up and east is to the left. Left: a 96 s *g*-band exposure with DECam. Right: a 30 s *z*-band exposure of the same field that reveals a great deal more stars than the longer exposure *g*-band observation.

Zhai et al. 2025), noting the dependence of microlensing event timescales on Galactic location. This work has highlighted how surveys of the plane can help characterize dark objects residing in the Galactic disk.

By mapping the microlensing event rates and characteristics throughout the Galactic bulge and plane, we can map the density of free-floating BHs as a function of Galactic longitude and latitude (see e.g., Wyrzykowski et al. 2016; Lam et al. 2020; Perkins et al. 2024), determine whether BHs and NSs receive kicks at formation (see e.g., Rose et al. 2022; Koshimoto et al. 2024), compare the mass functions and binary fractions of stars in different environments (see e.g., Wegg et al. 2017; Chabrier & Lenoble 2023; Abrams et al. 2025b), and determine whether planet occurrence depends on Galactic environment (see e.g., Penny et al. 2016; Koshimoto et al. 2021). While the planned 1 day cadence for the LS4 SOLE survey is not fast enough to fully characterize exoplanet events, targeted higher-cadence follow-up will enable measurements of the planetary properties (see e.g., Bachelet et al. 2024).

9.1.2. Off the Galactic Plane

The targeted discovery of microlensing events toward the bulge, M31, and Magellanic Clouds has been critical for constraining dark matter candidates and understanding the distribution of planets at large distances from their host star. The LS4 LEG and FOOT surveys, while generally focused away from regions of large optical depth to microlensing (i.e., away from the Galactic plane and Magellanic clouds), are highly favorable for the characterization of individual microlensing events. Departures on the order of a few days from single-lens curves due to planetary lensing will be readily detectable. Medford et al. (2023) identified 19 microlensing event candidates at $|b| \geqslant 10^{\circ}$ from the first three years of ZTF, almost doubling the number of events discovered in the stellar

halo. LS4 should similarly discover microlensing events away from the plane. The Einstein crossing time statistics of events off the plane can potentially constrain the contribution of primordial BHs to the dark matter mass fraction (Alcock et al. 1998; Green 2016; Mróz et al. 2025).

9.2. Other Galactic Science

Long-duration, high-cadence observations, such as those collected by CRTS and ZTF, have discovered many shortperiod (<90 minutes) systems (Drake et al. 2014; Ofek et al. 2020), including eclipsing dwarf novae, AM CVn stars (van Roestel et al. 2022), double degenerate systems (Coughlin et al. 2020) and below-the-period gap cataclysmic variables (CVs). We expect LS4 to uncover a bevy of such systems, including LISA verification binaries—those with well-constrained GW strain inferences (e.g., Kupfer et al. 2018). In addition to microlensing and GW follow-up, LS4 will enhance BH science by detecting optical counterparts to X-ray binaries (see e.g., Malzac et al. 2003). BHs and other compact objects with detached luminous companions can be detected via periodic optical signals from self-lensing, tidal ellipsoidal variation, and relativistic beaming (see e.g., Chawla et al. 2024; Nir & Bloom 2025).

As found in repeated Stripe 82 observations to $g \approx 21$ mag (Sesar et al. 2007), RR Lyrae can probe the inhomogeneous mass distribution (Vivas et al. 2001) of the outer halo of the Milky Way to $\sim 120\,\mathrm{kpc}$, revealing (due to the higher population density in the inner halo) $\sim 1.5\,\mathrm{kpc}$ substructure (such as tidal streams; Newberg et al. 2003) out to 30 kpc. Using RR Lyrae as probes, our understanding of the kinematics of the outer halo, inner halo and disk can be constrained by LS4 (e.g., Hernitschek et al. 2018; Iorio & Belokurov 2021; Medina et al. 2024).

10. Summary

In this paper we have described the design of the LS4 LEG, FOOT, and SOLE surveys, which will monitor the southern sky at cadences ranging from 1 to 3 days. The LS4 LEG survey will tile the extragalactic sky with a 3 days cadence to discover SNe Ia to be used in cosmological analyses, TDEs, AGN, and other rare transients. Nightly monitoring by the LS4 FOOT survey will reveal explosive transients in their infancy. The LS4 SOLE survey will map Galactic fields, primarily toward the bulge and inner plane, to find microlensing events and short-period binary systems. The LS4 partnership will also conduct ToO observations of GW events discovered by LVK and monitor the Euclid and ULTRASAT deep fields with the 10% of the observing time that is not part of the public survey.

The landscape of time-domain astronomy is rapidly evolving. Whereas one to two decades ago it was possible for individual collaborations to have a major impact with a single wide-field, optical telescope, modern efforts to identify

transients and variables must do so in an environment where several other telescopes are likely to be searching the same footprint on the sky. Later this year, any search or monitoring in the southern hemisphere will overlap LSST WFD observations, meaning smaller aperture surveys must compete and/or complement the deep, but at times sparse, observations from LSST. Furthermore, several wide-field transient surveys to be conducted outside the optical are planned or already underway, with projects like Einstein Probe (Yuan et al. 2018) monitoring the high-energy sky, the Karl G. Jansky Very Large Array Sky Survey (VLASS; Lacy et al. 2020) searching for radio transients, ULTRASAT and UVEX searching the UV, and Roman finding high-redshift transients with deep IR imaging. Taken together, we contend that future progress in the field will require clever strategies to complement the observations of other facilities and combine alerts from different surveys that span the EM spectrum. LS4 is an attempt to design such an experiment: while we have outlined a lot of science that LS4 can accomplish on its own, many of the most exciting science goals are directly the result of combining LS4 with substantially deeper surveys such as Rubin, Euclid, Roman, and ULTRASAT. Leveraging these disparate efforts affords LS4 the opportunity to have an outsized impact despite its modest (aperture) size.

Acknowledgments

This research used resources of the National Energy Research Scientific Computing Center (NERSC), a Department of Energy Office of Science User Facility using NERSC award HEP–ERCAP33561. P.E.N., R.A.K., K.W.L., and C.W. acknowledge support from the DOE/ASCR through DE-FOA-0001088, Analytical Modeling for Extreme-Scale Computing Environments, the X-SWAP Project.

A.A.M., C.L., and N.R. are supported by DoE award no. DE-SC0025599. La Silla Schmidt Southern Survey access for A.A. M., S.H., C.D.K., L.A.K., C.L., N.R., S.S., and V.S. was supported by Northwestern University and the Center for Interdisciplinary Exploration and Research in Astrophysics (CIERA). I.A. acknowledges support from the European Research Council (ERC) under the European Union's Horizon 2020 research and innovation program (grant agreement No. 852097), from the Israel Science Foundation (grant No. 2752/19), from the United States—Israel Binational Science Foundation (BSF; grant No. 2018166), and from the Pazy foundation (grant No. 216312). N.S.A. acknowledges support from the National Science Foundation under grant No. 1909641 and the Heising-Simons Foundation under grant No. 2022-3542. S.A. is supported by an LSST-DA Catalyst Fellowship (Grant 62192 from the John Templeton Foundation to LSST-DA). S.A. also gratefully acknowledges support from Stanford University, the United States Department of Energy, and a generous grant from Fred Kavli and The Kavli Foundation. D.B. is partially supported by a

NASA Future Investigators in NASA Earth and Space Science and Technology (FINESST) award no. 80NSSC23K1440. F.E.B. acknowledges support from ANID-Chile BASAL CATA FB210003, FONDECYT Regular 1241005, and Millennium Science Initiative, AIM23-0001. H.B. acknowledges the support by ANID BASAL Project 210003, ANID grant: Programa de Becas/Doctorado Nacional (21241862). Support for M.C. is provided by ANID's FONDECYT Regular grant No. 1231637; ANID's Millennium Science Initiative through grants ICN12 009 and AIM23-0001, awarded to the Millennium Institute of Astrophysics (MAS); and ANID's Basal project FB210003. A.F. and P.M.V. acknowledge the support from the DFG via the Collaborative Research Center SFB1491 Cosmic Interacting Matters—From Source to Signal. C.F. acknowledges support from STFC funding through grants ST/V002031/1, ST/ X00130X/1, and the Royal Society through grant IES\ R3\ 223075. A.G. acknowledges support from the Swedish Research Council, Dnr 2020-03444 and the Swedish National Space Agency, Dnr 2023-0022. C.P.G. acknowledges financial support from the Secretary of Universities and Research (Government of Catalonia) and by the Horizon 2020 Research and Innovation Programme of the European Union under the Marie Skłodowska-Curie and the Beatriu de Pinós 2021 BP 00168 programme, from the Spanish Ministerio de Ciencia e Innovación (MCIN) and the Agencia Estatal de Investigación (AEI) 10.13039/501100011033 under the PID2023-151307NB-100 SNNEXT project, from Centro Superior de Investigaciones Científicas (CSIC) under the PIE project 20215AT016 and the program Unidad de Excelencia María de Maeztu CEX2020-001058-M, and from the Departament de Recerca i Universitats de la Generalitat de Catalunya through the 2021-SGR-01270 grant. L.G. acknowledges financial support from the Spanish Ministerio de Ciencia e Innovación (MCIN) and the Agencia Estatal de Investigación (AEI) 10.13039/501100011033 under the PID2023-151307NB-I00 SNNEXT project, from Centro Superior de Investigaciones Científicas (CSIC) under projects PIE 20215AT016, ILINK23001, COOPB2304, and the program Unidad de Excelencia María de Maeztu CEX2020-001058-M, and from the Departament de Recerca i Universitats de la Generalitat de Catalunya through the 2021-SGR-01270 grant. I. H. gratefully acknowledges support from the Leverhulme Trust [International Fellowship IF-2023-027] and the UKRI Science and Technologies Facilities Council [grants ST/V000713/1 and ST/Y001230/1]. M.J.H. acknowledges support from the Heising-Simons Foundation under grant No. 2022-3542. S.H. was supported through a NASA grant awarded to the Illinois/NASA Space Grant Consortium. C.D.K. gratefully acknowledges support from the NSF through AST-2432037, the HST Guest Observer Program through HST-SNAP-17070 and HST-GO-17706, and from JWST Archival Research through JWST-AR-6241 and JWST-AR-5441. LAK is supported by a CIERA Postdoctoral Fellowship. R.L. acknowledges funding by the European Union (ERC, project no. 101042299, TransPIre).

Views and opinions expressed are however those of the author(s) only and do not necessarily reflect those of the European Union or the European Research Council Executive Agency. Neither the European Union nor the granting authority can be held responsible for them. J.R.L. acknowledges support from Heising-Simons Foundation Award no. 2022-3542. D.M. acknowledges support by ERC grant No. 833031 from the European Union. K.M. acknowledges funding from Horizon Europe ERC grant No. 101125877. L.M. acknowledges support through a UK Research and Innovation Future Leaders Fellowship (grant No. MR/T044136/1). R.M. acknowledges support by the National Science Foundation under award no. AST-2224255. M.N. is supported by the European Research Council (ERC) under the European Union's Horizon 2020 research and innovation programme (grant agreement No. 948381). G.P. acknowledges support from the National Agency for Research and Development (ANID) through the Millennium Science Initiative Program—ICN12 009. J.L.P. acknowledges support from ANID, Millennium Science Initiative, AIM23-0001. A.S. acknowledges support from the Knut and Alice Wallenberg foundation through the "Gravity Meets Light" project. B.D.S. acknowledges support through a UK Research and Innovation (UKRI) Future Leaders Fellowship [grant No. MR/T044136/1]. C.W.S. thanks Harvard University for support of this effort. G.P.S. acknowledges support from The Royal Society, the Leverhulme Trust, and the Science and Technology Facilities Council (grant No. ST/X001296/1). M.T.S. thanks the Israeli Science Foundation (grant Nos. 2068/22 and 2751/22). N.S. acknowledges support from the Knut and Alice Wallenberg Foundation through the "Gravity Meets Light" project and by and by the research environment grant "Gravitational Radiation and Electromagnetic Astrophysical Transients" (GREAT) funded by the Swedish Research Council (VR) under Dnr 2016-06012. B.T. acknowledges support from the European Research Council (ERC) under the European Union's Horizon 2020 research and innovation program (grant agreement No. 950533) and from the Israel Science Foundation (grant No. 1849/19). C.W. acknowledges support from the LSST Discovery Alliance under grant AWD1008640.

Fermi National Accelerator Laboratory (Fermilab) is a US Department of Energy, Office of Science, Office of High Energy Physics HEP User Facility. Fermilab is managed by FermiForward Discovery Group, LLC, acting under Contract no. 89243024CSC000002. This work was supported by the US Department of Energy (DOE), Office of Science, Office of High-Energy Physics, under contract no. DE-AC02-05CH11231. We gratefully acknowledge funding from ANID grants: Millennium Science Initiative—AIM23-0001 (FEB); CATA-BASAL—FB210003 (FEB); and FONDECYT Regular—1241005 (FEB). This research was funded in part by the Koret Foundation and by the Kavli Institute for Particle Astrophysics and Cosmology at Stanford University. This work was supported by ANID,

Millennium Science Initiative, AIM23-0001, and Centro de Modelamiento Matemático (CMM) BASAL fund FB210005.

The material contained in this document is based upon work partially supported by a National Aeronautics and Space Administration (NASA) grant or cooperative agreement. Any opinions, findings, conclusions, or recommendations expressed in this material are those of the author and do not necessarily reflect the views of NASA.

Major funding has been provided by the LS4 Founding Members: Northwestern University, Bar-Ilan University, Fermi National Accelerator Laboratory, Lawrence Berkeley National Laboratory, the Millenium Institute of Astrophysics, University of Portsmouth Higher Education Corporation, Tel Aviv University, The Regents of the University of California, Berkeley, and Yale University and the LS4 New Members: Purdue University. Project operations are covered by: DESY, IN2P3, Lancaster University, Ruhr-Universität - Bochum, Stockholm University, Trinity College Dublin, University of Southampton, Institute of Space Sciences (ICE, CSIC), Queen's University Belfast, and the University of Birmingham.

Facility: ESO:Schmidt.

Software: matplotlib (Hunter 2007), pandas (The pandas development team 2020), sncosmo (Barbary et al. 2016).

ORCID iDs

```
Adam A. Miller https://orcid.org/0000-0001-9515-478X
Natasha S. Abrams https://orcid.org/0000-0002-0287-3783
Shreya Anand https://orcid.org/0000-0003-3768-7515
Charlotte R. Angus https://orcid.org/0000-0002-4269-7999
Iair Arcavi  https://orcid.org/0000-0001-7090-4898
Charles Baltay https://orcid.org/0000-0003-0424-8719
Franz E. Bauer https://orcid.org/0000-0002-8686-8737
Daniel Brethauer  https://orcid.org/0000-0001-6415-0903
Joshua S. Bloom https://orcid.org/0000-0002-7777-216X
Hemanth Bommireddy https://orcid.org/0009-0007-4271-6444
Márcio Catelan https://orcid.org/0000-0001-6003-8877
Ryan Chornock https://orcid.org/0000-0002-7706-5668
Peter Clark  https://orcid.org/0000-0002-6576-7400
Thomas E. Collett https://orcid.org/0000-0001-5564-3140
Georgios Dimitriadis https://orcid.org/0000-0001-
9494-179X
Sara Faris https://orcid.org/0009-0007-8485-1281
Francisco Förster https://orcid.org/0000-0003-3459-2270
Anna Franckowiak https://orcid.org/0000-0002-5605-2219
Christopher Frohmaier https://orcid.org/0000-0001-9553-4723
Lluís Galbany https://orcid.org/0000-0002-1296-6887
Renato B. Galleguillos https://orcid.org/0000-0001-
6065-5218
Ariel Goobar  https://orcid.org/0000-0002-4163-4996
Or Graur https://orcid.org/0000-0002-4391-6137
Claudia P. Gutiérrez https://orcid.org/0000-0003-
```

2375-2064

```
Saarah Hall  https://orcid.org/0000-0002-3841-380X
Erica Hammerstein https://orcid.org/0000-0002-5698-8703
Kenneth R. Herner https://orcid.org/0000-0001-6718-2978
Isobel M. Hook https://orcid.org/0000-0002-2960-978X
Macy J. Huston https://orcid.org/0000-0003-4591-3201
Joel Johansson https://orcid.org/0000-0001-5975-290X
Charles D. Kilpatrick https://orcid.org/0000-0002-
5740-7747
Alex G. Kim https://orcid.org/0000-0001-6315-8743
Robert A. Knop  https://orcid.org/0000-0002-3803-1641
Marek P. Kowalski https://orcid.org/0000-0001-8594-8666
Lindsey A. Kwok https://orcid.org/0000-0003-3108-1328
Natalie LeBaron https://orcid.org/0000-0002-2249-0595
Kenneth W. Lin https://orcid.org/0000-0001-8967-2281
Chang Liu https://orcid.org/0000-0002-7866-4531
Jessica R. Lu https://orcid.org/0000-0001-9611-0009
Wenbin Lu https://orcid.org/0000-0002-1568-7461
Ragnhild Lunnan https://orcid.org/0000-0001-9454-4639
Kate Maguire https://orcid.org/0000-0002-9770-3508
Lydia Makrygianni https://orcid.org/0000-0002-7466-4868
Raffaella Margutti https://orcid.org/0000-0003-4768-7586
Patrik Milán Veres https://orcid.org/0000-0002-9553-2987
Thomas Moore https://orcid.org/0000-0001-8385-3727
A. J. Nayana https://orcid.org/0000-0002-8070-5400
Matt Nicholl https://orcid.org/0000-0002-2555-3192
Jakob Nordin https://orcid.org/0000-0001-8342-6274
S. R. Oates https://orcid.org/0000-0001-9309-7873
Giuliano Pignata https://orcid.org/0000-0003-0006-0188
Abigail Polin https://orcid.org/0000-0002-1633-6495
Dovi Poznanski https://orcid.org/0000-0003-1470-7173
Jose L. Prieto https://orcid.org/0000-0003-1072-2712
Nabeel Rehemtulla https://orcid.org/0000-0002-5683-2389
Mickael Rigault  https://orcid.org/0000-0002-8121-2560
Dan Ryczanowski https://orcid.org/0000-0002-4429-3429
Nikhil Sarin https://orcid.org/0000-0003-2700-1030
Steve Schulze https://orcid.org/0000-0001-6797-1889
Ved G. Shah https://orcid.org/0009-0009-1590-2318
Xinyue Sheng https://orcid.org/0000-0002-6527-1368
Samuel P. R. Shilling https://orcid.org/0009-0009-4622-7749
Brooke D. Simmons https://orcid.org/0000-0001-
5882-3323
Avinash Singh  https://orcid.org/0000-0003-2091-622X
Graham P. Smith https://orcid.org/0000-0003-4494-8277
Mathew Smith https://orcid.org/0000-0002-3321-1432
Jesper Sollerman https://orcid.org/0000-0003-1546-6615
Maayane T. Soumagnac https://orcid.org/0000-0001-
6753-1488
Christopher W. Stubbs https://orcid.org/0000-0003-
0347-1724
Mark Sullivan https://orcid.org/0000-0001-9053-4820
Aswin Suresh https://orcid.org/0009-0005-8230-030X
Benny Trakhtenbrot https://orcid.org/0000-0002-
3683-7297
```

```
Charlotte Ward https://orcid.org/0000-0002-4557-6682
Eli Wiston https://orcid.org/0009-0002-4843-2913
Yuhan Yao https://orcid.org/0000-0001-6747-8509
Peter E. Nugent https://orcid.org/0000-0002-3389-0586
```

References

```
Aartsen, M. G., Ackermann, M., Adams, J., et al. 2017a, JINST, 12, P03012
Aartsen, M. G., Ackermann, M., Adams, J., et al. 2017b, APh, 92, 30
Aartsen, M. G., Ackermann, M., Adams, J., et al. 2019, PhRvL, 122, 051102
Abbasi, R., Ackermann, M., Adams, J., et al. 2025, ApJ, 981, 159
Abbott, B. P., Abbott, R., Abbott, T. D., et al. 2017a, ApJL, 848, L12
Abbott, B. P., Abbott, R., Abbott, T. D., et al. 2017b, ApJL, 848, L13
Abbott, B. P., Abbott, R., Abbott, T. D., et al. 2017c, Natur, 551, 85
Abdurrahman, F. N., Stephens, H. F., & Lu, J. R. 2021, ApJ, 912, 146
Abrams, N. S., Hundertmark, M. P. G., Khakpash, S., et al. 2025a, ApJS,
Abrams, N. S., Lu, J. R., Lam, C. Y., et al. 2025b, ApJ, 980, 103
Adame, A. G., Aguilar, J., Ahlen, S., et al. 2025, JCAP, 2025, 021
Adrian-Martinez, S., Ageron, M., Aharonian, F., et al. 2016, JPhG, 43, 084001
Akeson, R., Armus, L., Bachelet, E., et al. 2019, arXiv:1902.05569
Alard, C., & Lupton, R. H. 1998, ApJ, 503, 325
Alcock, C., Allsman, R. A., Alves, D., et al. 1998, ApJL, 499, L9
Alcock, C., Allsman, R. A., Axelrod, T. S., et al. 1996, ApJ, 461, 84
Aleo, P. D., Malanchev, K., Sharief, S., et al. 2023, ApJS, 266, 9
Amanullah, R., Johansson, J., Goobar, A., et al. 2015, MNRAS, 453, 3300
Amanullah, R., Lidman, C., Rubin, D., et al. 2010, ApJ, 716, 712
Anderson, J. P., Pessi, P. J., Dessart, L., et al. 2018, A&A, 620, A67
Andreoni, I., Coughlin, M. W., Perley, D. A., et al. 2022a, Natur, 612, 430
Andreoni, I., Margutti, R., Salafia, O. S., et al. 2022b, ApJS, 260, 18
Andreoni, I., Margutti, R., Banovetz, J., et al. 2024, arXiv:2411.04793
Angus, C. R., Smith, M., Sullivan, M., et al. 2019, MNRAS, 487, 2215
Ansari, R., Cavalier, F., Moniez, M., et al. 1996, A&A, 314, 94
Arcavi, I., Gal-Yam, A., Sullivan, M., et al. 2014, ApJ, 793, 38
Arcavi, I., Howell, D. A., Kasen, D., et al. 2017a, Natur, 551, 210
Arcavi, I., McCully, C., Hosseinzadeh, G., et al. 2017b, ApJL, 848, L33
Arendse, N., Dhawan, S., Sagués Carracedo, A., et al. 2024, MNRAS,
  531, 3509
Bachelet, E., Rota, P., Bozza, V., et al. 2024, AJ, 168, 9
Baklanov, P. V., Sorokina, E. I., & Blinnikov, S. I. 2015, AstL, 41, 95
Baltay, C., Rabinowitz, D., Andrews, P., et al. 2007, PASP, 119, 1278
Baltay, C., Rabinowitz, D., Hadjiyska, E., et al. 2013, PASP, 125, 683
Barbary, K., Barclay, T., Biswas, R., et al., 2016 SNCosmo: Python Library
  for Supernova Cosmology, Astrophysics Source Code Library,
  ascl:1611.017
Barone-Nugent, R. L., Lidman, C., Wyithe, J. S. B., et al. 2012, MNRAS,
Bauer, F. E., Lira, P., Anguita, T., et al. 2023, Msngr, 190, 34
Bellm, E. C., Kulkarni, S. R., Barlow, T., et al. 2019a, PASP, 131, 068003
Bellm, E. C., Kulkarni, S. R., Graham, M. J., et al. 2019b, PASP, 131, 018002
Bersten, M. C., Benvenuto, O. G., Nomoto, K., et al. 2012, ApJ, 757, 31
Bertin, E., & Arnouts, S. 1996, A&AS, 117, 393
Betoule, M., Kessler, R., Guy, J., et al. 2014, A&A, 568, A22
Bhat, P. N., Meegan, C. A., von Kienlin, A., et al. 2016, ApJS, 223, 28
Bianco, F. B., Ivezić, Ž., Jones, R. L., et al. 2022, ApJS, 258, 1
Bildsten, L., Shen, K. J., Weinberg, N. N., & Nelemans, G. 2007, ApJL,
  662, L95
Birrer, S., Smith, G. P., Shajib, A. J., Ryczanowski, D., & Arendse, N. 2025,
         A. 383, 20240130
Blinnikov, S. I., & Sorokina, E. I. 2010, arXiv:1009.4353
Bloemen, S., Groot, P., Woudt, P., et al. 2016, Proc. SPIE, 9906, 990664
Bloom, J. S., Richards, J. W., Nugent, P. E., et al. 2012, PASP, 124, 1175
Bocchio, M., Marassi, S., Schneider, R., et al. 2016, A&A, 587, A157
Bohlin, R. C., Hubeny, I., & Rauch, T. 2020, AJ, 160, 21
Boian, I., & Groh, J. H. 2020, MNRAS, 496, 1325
Boone, K., Aldering, G., Antilogus, P., et al. 2021, ApJ, 912, 71
Borucki, W. J., Koch, D., Basri, G., et al. 2010, Sci, 327, 977
Bose, S., Dong, S., Pastorello, A., et al. 2018, ApJ, 853, 57
```

```
Botticella, M. T., Pastorello, A., Smartt, S. J., et al. 2009, MNRAS, 398, 1041
Bowen, I. S. 1934, PASP, 46, 146
Boyd, B. M., Narayan, G., Mandel, K. S., et al. 2025, MNRAS, 540, 385
Brout, D., Sako, M., Scolnic, D., et al. 2019, ApJ, 874, 106
Brout, D., & Scolnic, D. 2021, ApJ, 909, 26
Brout, D., Scolnic, D., Popovic, B., et al. 2022, ApJ, 938, 110
Brown, T. M., Baliber, N., Bianco, F. B., et al. 2013, PASP, 125, 1031
Bruch, R. J., Gal-Yam, A., Schulze, S., et al. 2021, ApJ, 912, 46
Bruch, R. J., Gal-Yam, A., Yaron, O., et al. 2023, ApJ, 952, 119
Buchdahl, H. A. 1970, MNRAS, 150, 1
Burke, J., Howell, D. A., Sarbadhicary, S. K., et al. 2021, ApJ, 919, 142
Burrows, D. N., Kennea, J. A., Ghisellini, G., et al. 2011, Natur, 476, 421
Cao, Y., Kulkarni, S. R., Howell, D. A., et al. 2015, Natur, 521, 328
Cenko, S. B., Bloom, J. S., Kulkarni, S. R., et al. 2012, MNRAS, 420, 2684
Chabrier, G., & Lenoble, R. 2023, ApJL, 944, L33
Charisi, M., Bartos, I., Haiman, Z., et al. 2016, MNRAS, 463, 2145
Chawla, C., Chatterjee, S., Shah, N., & Breivik, K. 2024, ApJ, 975, 163
Chen, P., Gal-Yam, A., Sollerman, J., et al. 2024, Natur, 625, 253
Chen, T. W., Inserra, C., Fraser, M., et al. 2018, ApJL, 867, L31
Chen, T.-W., Smartt, S. J., Yates, R. M., et al. 2017, MNRAS, 470, 3566
Chen, W., Kelly, P. L., Oguri, M., et al. 2022, Natur, 611, 256
Chen, Z., & Ivanova, N. 2024, ApJL, 963, L35
Chen, Z. H., Yan, L., Kangas, T., et al. 2023a, ApJ, 943, 41
Chen, Z. H., Yan, L., Kangas, T., et al. 2023b, ApJ, 943, 42
Childress, M., Aldering, G., Antilogus, P., et al. 2013, ApJ, 770, 108
Connaughton, V., Burns, E., Goldstein, A., et al. 2016, ApJL, 826, L6
Coppejans, D. L., Margutti, R., Terreran, G., et al. 2020, ApJL, 895, L23
Coughlin, M. W., Burdge, K., Phinney, E. S., et al. 2020, MNRAS, 494, L91
Coulter, D. A., Foley, R. J., Kilpatrick, C. D., et al. 2017, Sci, 358, 1556
Cowperthwaite, P. S., Berger, E., Villar, V. A., et al. 2017, ApJL, 848, L17
Dai, L., McKinney, J. C., Roth, N., Ramirez-Ruiz, E., & Miller, M. C. 2018,
   ApJL, 859, L20
Dark Energy Survey Collaboration, Abbott, T., Abdalla, F. B., et al. 2016,
        RAS, 460, 1270
Das, K. K., Kasliwal, M. M., Sollerman, J., et al. 2024, ApJ, 972, 91
Davis, T. M., Hui, L., Frieman, J. A., et al. 2011, ApJ, 741, 67
De, K., Kasliwal, M. M., Polin, A., et al. 2019, ApJL, 873, L18
De, K., Kasliwal, M. M., Tzanidakis, A., et al. 2020, ApJ, 905, 58
De Cia, A., Gal-Yam, A., Rubin, A., et al. 2018, ApJ, 860, 100
De Colle, F., & Lu, W. 2020, NewAR, 89, 101538
de Jaeger, T., & Galbany, L. 2024, in The Hubble Constant Tension, ed.
   E. Di Valentino & D. Brout (Singapore: Springer), 177
de Jaeger, T., Galbany, L., Riess, A. G., et al. 2022, MNRAS, 514, 4620
de Jaeger, T., Stahl, B. E., Zheng, W., et al. 2020, MNRAS, 496, 3402
de Jong, R. S., Agertz, O., Berbel, A. A., et al. 2019, Msngr, 175, 3
Deckers, M., Maguire, K., Magee, M. R., et al. 2022, MNRAS, 512, 1317
DES Collaboration, Abbott, T. M. C., Acevedo, M., et al. 2024, ApJL,
   973, L14
DESI Collaboration, Aghamousa, A., Aguilar, J., et al. 2016, arXiv:1611.
   00036
Dhawan, S., Bulla, M., Goobar, A., Sagués Carracedo, A., & Setzer, C. N.
   2020, ApJ, 888, 67
Dimitriadis, G., Foley, R. J., Rest, A., et al. 2019, ApJL, 870, L1
Djorgovski, S. G., Baltay, C., Mahabal, A. A., et al. 2008, AN, 329, 263
Dong, Y., Valenti, S., Polin, A., et al. 2022, ApJ, 934, 102
Drake, A. J., Djorgovski, S. G., García-Álvarez, D., et al. 2014, ApJ, 790, 157
Drake, A. J., Djorgovski, S. G., Mahabal, A., et al. 2009, ApJ, 696, 870
Drout, M. R., Chornock, R., Soderberg, A. M., et al. 2014, ApJ, 794, 23
Drout, M. R., Piro, A. L., Shappee, B. J., et al. 2017, Sci, 358, 1570
Dvali, G., Gabadadze, G., & Porrati, M. 2000, PhLB, 485, 208
Euclid Collaboration, Moneti, A., McCracken, H. J., et al. 2022a, A&A,
   658, A126
Euclid Collaboration, Scaramella, R., Amiaux, J., et al. 2022b, A&A,
   662, A112
Fang, K., Metzger, B. D., Vurm, I., Aydi, E., & Chomiuk, L. 2020, ApJ, 904, 4
Faris, S., Arcavi, I., Makrygianni, L., et al. 2024, ApJ, 969, 104
Filippenko, A. V. 1997, ARA&A, 35, 309
Flaugher, B. L., Abbott, T. M. C., Angstadt, R., et al. 2012, Proc. SPIE,
Foley, R. J. 2015, MNRAS, 452, 2463
```

```
Förster, F., Cabrera-Vives, G., Castillo-Navarrete, E., et al. 2021, AJ, 161, 242
Foucart, F., Hinderer, T., & Nissanke, S. 2018, PhRvD, 98, 081501
Frederick, S., Gezari, S., Graham, M. J., et al. 2021, ApJ, 920, 56
Freedman, W. L., & Madore, B. F. 2023, JCAP, 2023, 050
Freedman, W. L., Madore, B. F., Hoyt, T. J., et al. 2025, ApJ, 985, 203
French, K. D., Arcavi, I., & Zabludoff, A. 2016, ApJL, 818, L21
French, K. D., Wevers, T., Law-Smith, J., Graur, O., & Zabludoff, A. I. 2020,
     SRv. 216, 32
Frieman, J. A., Bassett, B., Becker, A., et al. 2008, AJ, 135, 338
Frohmaier, C., Vincenzi, M., Sullivan, M., et al. 2025, arXiv:2501.16311
Frye, B. L., Pascale, M., Pierel, J., et al. 2024, ApJ, 961, 171
Gaia Collaboration, Vallenari, A., Brown, A. G. A., et al. 2023, A&A, 674, A1
Gal-Yam, A. 2017, in Handbook of Supernovae, ed. A. W. Alsabti &
  P. Murdin (Cham: Springer), 195
Gal-Yam, A. 2019, ARA&A, 57, 305
Gal-Yam, A., Arcavi, I., Ofek, E. O., et al. 2014, Natur, 509, 471
Gal-Yam, A., Bruch, R., Schulze, S., et al. 2022, Natur, 601, 201
Garnavich, P., Wood, C. M., Milne, P., et al. 2023, ApJ, 953, 35
Gezari, S. 2021, ARA&A, 59, 21
Gezari, S., Hung, T., Cenko, S. B., et al. 2017, ApJ, 835, 144
Ginolin, M., Rigault, M., Copin, Y., et al. 2025, A&A, 694, A4
Goldstein, D. A., Nugent, P. E., & Goobar, A. 2019, ApJS, 243, 6
Goobar, A., Amanullah, R., Kulkarni, S. R., et al. 2017, Sci, 356, 291
Goobar, A., Johansson, J., Schulze, S., et al. 2023, NatAs, 7, 1098
Goobar, A., Kromer, M., Siverd, R., et al. 2015, ApJ, 799, 106
Goobar, A., & Leibundgut, B. 2011, ARNPS, 61, 251
Goyal, S., Haris, K., Mehta, A. K., & Ajith, P. 2021, PhRvD, 103, 024038
Graham, M. J., Djorgovski, S. G., Stern, D., et al. 2015a, Natur, 518, 74
Graham, M. J., Djorgovski, S. G., Stern, D., et al. 2015b, MNRAS, 453, 1562
Graham, M. J., Ford, K. E. S., McKernan, B., et al. 2020, PhRvL, 124, 251102
Graham, M. L., Harris, C. E., Nugent, P. E., et al. 2019, ApJ, 871, 62
Graham, M. L., Knop, R. A., Kennedy, T. D., et al. 2023, MNRAS, 519, 3881
Graur, O. 2019, ApJ, 870, 14
Graur, O., Maguire, K., Ryan, R., et al. 2020, NatAs, 4, 188
Graur, O., Zurek, D., Shara, M. M., et al. 2016, ApJ, 819, 31
Grayling, M., Thorp, S., Mandel, K. S., et al. 2024, MNRAS, 531, 953
Green, A. M. 2016, PhRvD, 94, 063530
Greene, J. E., Strader, J., & Ho, L. C. 2020, ARA&A, 58, 257
Groh, J. H. 2014, A&A, 572, L11
Groot, P. J., Bloemen, S., Vreeswijk, P. M., et al. 2024, PASP, 136, 115003
Guo, H., Sun, J., Li, S., et al. 2025, ApJ, 979, 235
Gutiérrez, C. P., Bersten, M. C., Orellana, M., et al. 2021, MNRAS, 504, 4907
Hammerstein, E., Cenko, S. B., Gezari, S., et al. 2023a, ApJ, 957, 86
Hammerstein, E., Cenko, S. B., Andreoni, I., et al. 2025, arXiv:2506.08250
Hammerstein, E., Gezari, S., van Velzen, S., et al. 2021, ApJL, 908, L20
Hammerstein, E., van Velzen, S., Gezari, S., et al. 2023b, ApJ, 942, 9
Hamuy, M., & Pinto, P. A. 2002, ApJL, 566, L63
Hernitschek, N., Cohen, J. G., Rix, H.-W., et al. 2018, ApJ, 859, 31
Hinkle, J. T. 2024, MNRAS, 531, 2603
Hinkle, J. T., Holoien, T. W. S., Shappee, B. J., et al. 2022, ApJ, 930, 12
Hinkle, J. T., Kochanek, C. S., Shappee, B. J., et al. 2023, MNRAS, 521, 3517
Hirata, K., Kajita, T., Koshiba, M., et al. 1987, PhRvL, 58, 1490
Hjorth, J., Levan, A. J., Tanvir, N. R., et al. 2017, ApJL, 848, L31
Ho, A. Y. Q., Perley, D. A., Yao, Y., et al. 2022, ApJ, 938, 85
Ho, A. Y. Q., Yao, Y., Matsumoto, T., et al. 2025, ApJ, 989, 54
Holoien, T. W. S., Neustadt, J. M. M., Vallely, P. J., et al. 2022, ApJ, 933, 196
Holtzman, J. A., Hester, J. J., Casertano, S., et al. 1995, PASP, 107, 156
Horiuchi, S., & Ando, S. 2008, PhRvD, 77, 063007
Hosseinzadeh, G., Berger, E., Metzger, B. D., et al. 2022, ApJ, 933, 14
Hosseinzadeh, G., Sand, D. J., Valenti, S., et al. 2017, ApJL, 845, L11
Howlett, C., Robotham, A. S. G., Lagos, C. D. P., & Kim, A. G. 2017, ApJ,
Huang, S., Jiang, N., Zhu, J., et al. 2024, ApJL, 964, L22
Huang, X., Davis, S. W., Jiang, Y.-f., et al. 2024, ApJ, 974, 165
Huang, X., Raha, Z., Aldering, G., et al. 2017, ApJ, 836, 157
Hui, L., & Greene, P. B. 2006, PhRvD, 73, 123526
Hunter, J. D. 2007, CSE, 9, 90
IceCube Collaboration 2013, Sci, 342, 1242856
IceCube Collaboration, Aartsen, M. G., Ackermann, M., et al. 2018a, Sci, 361,
```

```
361, 147
IceCube Collaboration, Aartsen, M. G., Abraham, K., et al. 2016, JINST, 11,
   P11009
IceCube Collaboration, Abbasi, R., Ackermann, M., et al. 2022, Sci, 378,
Icecube Collaboration, Abbasi, R., Ackermann, M., et al. 2023, Sci, 380, 1338
Iorio, G., & Belokurov, V. 2021, MNRAS, 502, 5686
Ivezić, Ž., Kahn, S. M., Tyson, J. A., et al. 2019, ApJ, 873, 111
Jacobson-Galán, W. V., Dessart, L., Davis, K. W., et al. 2024, ApJ, 970, 189
Jacobson-Galán, W. V., Dessart, L., Jones, D. O., et al. 2022a, ApJ, 924, 15
Jacobson-Galán, W. V., Dimitriadis, G., Foley, R. J., & Kilpatrick, C. D. 2018,
   ApJ, 857, 88
Jacobson-Galán, W. V., Margutti, R., Kilpatrick, C. D., et al. 2020a, ApJ,
   898, 166
Jacobson-Galán, W. V., Polin, A., Foley, R. J., et al. 2020b, ApJ, 896, 165
Jacobson-Galán, W. V., Venkatraman, P., Margutti, R., et al. 2022b, ApJ,
   932, 58
Jencson, J. E., Adams, S. M., Bond, H. E., et al. 2019, ApJL, 880, L20
Jiang, J.-A., Doi, M., Maeda, K., et al. 2017a, Natur, 550, 80
Jiang, N., Wang, T., Yan, L., et al. 2017b, ApJ, 850, 63
Johansson, J., Cenko, S. B., Fox, O. D., et al. 2021, ApJ, 923, 237
Jones, D. O., Foley, R. J., Narayan, G., et al. 2021, ApJ, 908, 143
Jones, L. 2022, Calculating LSS. Limiting Magnitudes and SNR, Vera C.
   Rubin Observatory, https://smtn-002.lsst.io/
Kaiser, N., Burgett, W., Chambers, K., et al. 2010, Proc. SPIE, 7733, 77330E
Kangas, T., Kuncarayakti, H., Nagao, T., et al. 2024, A&A, 689, A182
Kasen, D. 2006, ApJ, 649, 939
Kasen, D. 2010, ApJ, 708, 1025
Kasen, D., & Bildsten, L. 2010, ApJ, 717, 245
Kasliwal, M. M., Bally, J., Masci, F., et al. 2017a, ApJ, 839, 88
Kasliwal, M. M., Kulkarni, S. R., Arcavi, I., et al. 2011, ApJ, 730, 134
Kasliwal, M. M., Kulkarni, S. R., Gal-Yam, A., et al. 2012, ApJ, 755, 161
Kasliwal, M. M., Nakar, E., Singer, L. P., et al. 2017b, Sci, 358, 1559
Kawabata, K. S., Maeda, K., Nomoto, K., et al. 2010, Natur, 465, 326
Keller, S. C., Schmidt, B. P., Bessell, M. S., et al. 2007, PASA, 24, 1
Kelly, P., Zitrin, A., Oguri, M., et al. 2022, TNSAN, 169, 1
Kelly, P. L., Hicken, M., Burke, D. L., Mandel, K. S., & Kirshner, R. P. 2010,
      J, 715, 743
Kelly, P. L., Rodney, S. A., Treu, T., et al. 2015, Sci, 347, 1123
Khatami, D. K., & Kasen, D. N. 2024, ApJ, 972, 140
Kiendrebeogo, R. W., Farah, A. M., Foley, E. M., et al. 2023, ApJ, 958, 158
Kiewe, M., Gal-Yam, A., Arcavi, I., et al. 2012, ApJ, 744, 10
Kim, A. G., & Linder, E. V. 2020, PhRvD, 101, 023516
Kim, D. J., Kim, H. W., Hwang, K. H., et al. 2018, AJ, 155, 76
Kimura, S. S. 2023, in The Encyclopedia of Cosmology. Set 2: Frontiers in
   Cosmology. Volume 2: Neutrino Physics and Astrophysics, ed.
   F. W. Stecker (World Scientific Publishing Co. Pte. Ltd.), 433
Kirshner, R. P., & Kwan, J. 1974, ApJ, 193, 27
KM3NeT Collaboration, Aiello, S., Albert, A., et al. 2025, Natur, 638, 376
Kollmeier, J., Anderson, S. F., Blanc, G. A., et al. 2019, BAAS, 51, 274
Koshimoto, N., Bennett, D. P., Suzuki, D., & Bond, I. A. 2021, ApJL, 918, L8
Koshimoto, N., Kawanaka, N., & Tsuna, D. 2024, ApJ, 973, 5
Kulkarni, S. R., Harrison, F. A., Grefenstette, B. W., et al. 2021, arXiv:2111.
Kuncarayakti, H., Sollerman, J., Izzo, L., et al. 2023, A&A, 678, A209
Kupfer, T., Korol, V., Shah, S., et al. 2018, MNRAS, 480, 302
Lacy, M., Baum, S. A., Chandler, C. J., et al. 2020, PASP, 132, 035001
Laha, S., Meyer, E., Roychowdhury, A., et al. 2022, ApJ, 931, 5
Lam, C. Y. 2023, PhD thesis, University of California, Berkeley https://www.
   proquest.com/dissertations-theses/understanding-galactic-black-hole-
   population-with/docview/2866322369/se-2
Lam, C. Y., & Lu, J. R. 2023, ApJ, 955, 116
Lam, C. Y., Lu, J. R., Hosek, M. W., Jr., Dawson, W. A., & Golovich, N. R.
   2020, ApJ, 889, 31
Larison, C., Jha, S. W., Kwok, L. A., & Camacho-Neves, Y. 2024, ApJ,
   961, 185
Larson, S., Beshore, E., Hill, R., et al. 2003, BAAS, 35, 982
Law, N. M., Fors, O., Ratzloff, J., et al. 2015, PASP, 127, 234
Law, N. M., Kulkarni, S. R., Dekany, R. G., et al. 2009, PASP, 121, 1395
```

IceCube Collaboration, Aartsen, M. G., Ackermann, M., et al. 2018b, Sci,

```
Law-Smith, J., Ramirez-Ruiz, E., Ellison, S. L., & Foley, R. J. 2017, ApJ,
Leloudas, G., Chatzopoulos, E., Dilday, B., et al. 2012, A&A, 541, A129
Leloudas, G., Schulze, S., Krühler, T., et al. 2015, MNRAS, 449, 917
Leonard, D. C., Filippenko, A. V., Gates, E. L., et al. 2002, PASP, 114, 35
Li, J., Wang, Z., & Zheng, D. 2023, MNRAS, 522, 2928
Linder, E. V. 2013, JCAP, 2013, 031
Linder, E. V., & Cahn, R. N. 2007, APh, 28, 481
Lipunov, V. M., Gorbovskoy, E., Kornilov, V. G., et al. 2017, ApJL, 850, L1
Liu, C., Miller, A. A., Boos, S. J., et al. 2023a, ApJ, 958, 178
Liu, C., Miller, A. A., Polin, A., et al. 2023b, ApJ, 946, 83
Liu, T., Gezari, S., Burgett, W., et al. 2016, ApJ, 833, 6
LSST Science Collaboration, Abell, P. A., Allison, J., et al. 2009,
   arXiv:0912.0201
Lu, J. R., Sinukoff, E., Ofek, E. O., Udalski, A., & Kozlowski, S. 2016, ApJ,
   830, 41
Lu, W., & Bonnerot, C. 2020, MNRAS, 492, 686
Lunnan, R., Chornock, R., Berger, E., et al. 2014, ApJ, 787, 138
Lunnan, R., Chornock, R., Berger, E., et al. 2018a, ApJ, 852, 81
Lunnan, R., Fransson, C., Vreeswijk, P. M., et al. 2018b, NatAs, 2, 887
Lunnan, R., Kasliwal, M. M., Cao, Y., et al. 2017, ApJ, 836, 60
Lyman, J. D., Levan, A. J., Church, R. P., Davies, M. B., & Tanvir, N. R.
   2014, MNRAS, 444, 2157
MacLeod, C. L., Ross, N. P., Lawrence, A., et al. 2016, MNRAS, 457, 389
Magare, S., Kapadia, S. J., More, A., et al. 2023, ApJL, 955, L31
Magee, M. R., & Maguire, K. 2020, A&A, 642, A189
Malzac, J., Belloni, T., Spruit, H. C., & Kanbach, G. 2003, A&A, 407, 335
Mandel, K. S., Scolnic, D. M., Shariff, H., Foley, R. J., & Kirshner, R. P.
   2017, ApJ, 842, 93
Mandel, K. S., Thorp, S., Narayan, G., Friedman, A. S., & Avelino, A. 2022,
   MNRAS, 510, 3939
Margutti, R., & Chornock, R. 2021, ARA&A, 59, 155
Margutti, R., Cowperthwaite, P., Doctor, Z., et al. 2018, arXiv:1812.04051
Margutti, R., Milisavljevic, D., Soderberg, A. M., et al. 2014, ApJ, 780, 21
Matheson, T., Stubens, C., Wolf, N., et al. 2021, AJ, 161, 107
Mauerhan, J. C., Smith, N., Filippenko, A. V., et al. 2013, MNRAS, 430,
Medford, M. S., Abrams, N. S., Lu, J. R., Nugent, P., & Lam, C. Y. 2023, ApJ,
   947, 24
Medina, G. E., Muñoz, R. R., Carlin, J. L., et al. 2024, MNRAS, 531, 4762
Meegan, C., Lichti, G., Bhat, P. N., et al. 2009, ApJ, 702, 791
Melchior, P., Moolekamp, F., Jerdee, M., et al. 2018, A&C, 24, 129
Mészáros, P., & Waxman, E. 2001, PhRvL, 87, 171102
Metzger, B. D., Bauswein, A., Goriely, S., & Kasen, D. 2015, MNRAS,
   446, 1115
Milisavljevic, D., Margutti, R., Kamble, A., et al. 2015, ApJ, 815, 120
Milisavljevic, D., Patnaude, D. J., Raymond, J. C., et al. 2017, ApJ, 846, 50
Miller, A. A., Magee, M. R., Polin, A., et al. 2020, ApJ, 898, 56
Millon, M., Michalewicz, K., Dux, F., Courbin, F., & Marshall, P. J. 2024, AJ,
Möller, A., Peloton, J., Ishida, E. E. O., et al. 2021, MNRAS, 501, 3272
Moore, T., Smartt, S. J., Nicholl, M., et al. 2023, ApJL, 956, L31
Moriya, T. J., & Eldridge, J. J. 2016, MNRAS, 461, 2155
Moriya, T. J., Maeda, K., Taddia, F., et al. 2013, MNRAS, 435, 1520
Moriya, T. J., Sorokina, E. I., & Chevalier, R. A. 2018, SSRv, 214, 59
Morozova, V., Piro, A. L., & Valenti, S. 2018, ApJ, 858, 15
Mróz, P., Street, R. A., Bachelet, E., et al. 2020, RNAAS, 4, 13
Mróz, P., Udalski, A., Szymański, M. K., et al. 2025, ApJS, 280, 49
Mummery, A., van Velzen, S., Nathan, E., et al. 2024, MNRAS, 527, 2452
Munari, U., Henden, A., Kiyota, S., et al. 2002, A&A, 389, L51
Murase, K. 2018, PhRvD, 97, 081301
Murase, K., Franckowiak, A., Maeda, K., Margutti, R., & Beacom, J. F. 2019,
   ApJ, 874, 80
Murase, K., & Ioka, K. 2013, PhRvL, 111, 121102
Murase, K., Thompson, T. A., Lacki, B. C., & Beacom, J. F. 2011, PhRvD, 84,
  043003
Nakar, E. 2015, ApJ, 807, 172
Nandez, J. L. A., Ivanova, N., & Lombardi, J. C., Jr. 2014, ApJ, 786, 39
Newberg, H. J., Yanny, B., Grebel, E. K., et al. 2003, ApJL, 596, L191
Nicholl, M., & Andreoni, I. 2025, RSPTA, 383, 20240126
```

```
Nicholl, M., Berger, E., Margutti, R., et al. 2016, ApJL, 828, L18
Nicholl, M., & Smartt, S. J. 2016, MNRAS, 457, L79
Nicholl, M., Smartt, S. J., Jerkstrand, A., et al. 2015, MNRAS, 452, 3869
Niemela, V. S., Ruiz, M. T., & Phillips, M. M. 1985, ApJ, 289, 52
Nir, G., & Bloom, J. S. 2025, ApJ, 978, 169
Noebauer, U. M., Kromer, M., Taubenberger, S., et al. 2017, MNRAS,
  472, 2787
Nomoto, K. 1984, ApJ, 277, 791
Nordin, J., Brinnel, V., van Santen, J., et al. 2019, A&A, 631, A147
Nugent, P., & Hamuy, M. 2017, in Cosmology with Type IIP Supernovae, ed.
   A. W. Alsabti & P. Murdin (Cham: Springer), 2671
Nugent, P., Sullivan, M., Ellis, R., et al. 2006, ApJ, 645, 841
Nugent, P. E., Sullivan, M., Cenko, S. B., et al. 2011, Natur, 480, 344
Nyholm, A., Sollerman, J., Tartaglia, L., et al. 2020, A&A, 637, A73
Nyland, K., Dong, D. Z., Patil, P., et al. 2020, ApJ, 905, 74
Oates, S. R., Kuin, N. P. M., Nicholl, M., et al. 2024, MNRAS, 530, 1688
Ofek, E. O., Soumagnac, M., Nir, G., et al. 2020, MNRAS, 499, 5782
Ofek, E. O., Sullivan, M., Shaviv, N. J., et al. 2014, ApJ, 789, 104
Oguri, M., & Marshall, P. J. 2010, MNRAS, 405, 2579
Olivares, E. F., Hamuy, M., Pignata, G., et al. 2010, ApJ, 715, 833
Padilla Gonzalez, E., Howell, D. A., Burke, J., et al. 2023, ApJ, 953, 25
Palmese, A., Graur, O., Annis, J. T., et al. 2019, BAAS, 51, 310
Pastorello, A., Fraser, M., Valerin, G., et al. 2021, A&A, 646, A119
Penny, M. T., Henderson, C. B., & Clanton, C. 2016, ApJ, 830, 150
Perets, H. B., Gal-Yam, A., Mazzali, P. A., et al. 2010, Natur, 465, 322
Perkins, S. E., McGill, P., Dawson, W., et al. 2024, ApJ, 961, 179
Perley, D. A., Fremling, C., Sollerman, J., et al. 2020, ApJ, 904, 35
Perley, D. A., Quimby, R. M., Yan, L., et al. 2016, ApJ, 830, 13
Perlmutter, S., Aldering, G., Goldhaber, G., et al. 1999, ApJ, 517, 565
Perlmutter, S., Gabi, S., Goldhaber, G., et al. 1997, ApJ, 483, 565
Petropoulou, M., Coenders, S., Vasilopoulos, G., Kamble, A., & Sironi, L.
  2017, MNRAS, 470, 1881
Petrushevska, T., Leloudas, G., Ilić, D., et al. 2023, A&A, 669, A140
Phillips, M. M. 1993, ApJL, 413, L105
Pierel, J. D. R., Frye, B. L., Pascale, M., et al. 2024, ApJ, 967, 50
Piran, T., Svirski, G., Krolik, J., Cheng, R. M., & Shiokawa, H. 2015, ApJ,
   806, 164
Piro, A. L. 2012, ApJ, 759, 83
Piro, A. L. 2015, ApJL, 808, L51
Piro, A. L., & Kollmeier, J. A. 2018, ApJ, 855, 103
Piro, A. L., & Morozova, V. S. 2016, ApJ, 826, 96
Planck Collaboration, Aghanim, N., Akrami, Y., et al. 2020, A&A, 641, A6
Pojmański, G. 1997, AcA, 47, 467
Polin, A., Nugent, P., & Kasen, D. 2019, ApJ, 873, 84
Prentice, S. J., Ashall, C., James, P. A., et al. 2019, MNRAS, 485, 1559
Quimby, R. M., De Cia, A., Gal-Yam, A., et al. 2018, ApJ, 855, 2
Quimby, R. M., Kulkarni, S. R., Kasliwal, M. M., et al. 2011, Natur, 474, 487
Quimby, R. M., Werner, M. C., Oguri, M., et al. 2013, ApJL, 768, L20
Rabinowitz, D., Schwamb, M. E., Hadjiyska, E., & Tourtellotte, S. 2012, AJ,
   144, 140
Ramsden, P., Nicholl, M., McGee, S. L., & Mummery, A. 2025, MNRAS,
  541, 1218
Rayoux, C., Carreres, B., Rosselli, D., et al. 2025, A&A, 698, 273
Razzaque, S., Mészáros, P., & Waxman, E. 2005, PhRvL, 94, 109903
Rees, M. J. 1988, Natur, 333, 523
Rehemtulla, N., Jacobson-Galán, W. V., Singh, A., et al. 2025, ApJ, 985, 241
Rehemtulla, N., Miller, A. A., Jegou Du Laz, T., et al. 2024, ApJ, 972, 7
Reusch, S., Stein, R., Kowalski, M., et al. 2022, PhRvL, 128, 221101
Ricci, C., Kara, E., Loewenstein, M., et al. 2020, ApJL, 898, L1
Ricci, C., & Trakhtenbrot, B. 2023, NatAs, 7, 1282
Richmond, M. W., Filippenko, A. V., & Galisky, J. 1998, PASP, 110, 553
Riess, A. G., Casertano, S., Yuan, W., Macri, L. M., & Scolnic, D. 2019, ApJ,
Riess, A. G., Filippenko, A. V., Challis, P., et al. 1998, AJ, 116, 1009
Riess, A. G., Press, W. H., & Kirshner, R. P. 1996, ApJ, 473, 88
Riess, A. G., Yuan, W., Macri, L. M., et al. 2022, ApJL, 934, L7
Rigault, M., Brinnel, V., Aldering, G., et al. 2020, A&A, 644, A176
Rigault, M., Copin, Y., Aldering, G., et al. 2013, A&A, 560, A66
Rigault, M., Smith, M., Regnault, N., et al. 2025, A&A, 694, A2
Robertson, A., Smith, G. P., Massey, R., et al. 2020, MNRAS, 495, 3727
```

```
Rodney, S. A., Brammer, G. B., Pierel, J. D. R., et al. 2021, NatAs, 5, 1118
Rodriguez, A. C., Mróz, P., Kulkarni, S. R., et al. 2022, ApJ, 927, 150
Rodriguez, C., Taylor, G. B., Zavala, R. T., et al. 2006, ApJ, 646, 49
Rose, S., Lam, C. Y., Lu, J. R., et al. 2022, ApJ, 941, 116
Rosselli, D., Carreres, B., Ravoux, C., et al. 2025, A&A, 701, A119
Rubin, D., Aldering, G., Barbary, K., et al. 2015, ApJ, 813, 137
Rubin, D., Aldering, G., Betoule, M., et al. 2025, ApJ, 986, 231
Sahu, K. C., Anderson, J., Casertano, S., et al. 2022, ApJ, 933, 83
Said, K., Howlett, C., Davis, T., et al. 2025, MNRAS, 539, 3627
Sainz de Murieta, A., Collett, T. E., Magee, M. R., et al. 2023, MNRAS,
  526, 4296
Sainz de Murieta, A., Collett, T. E., Magee, M. R., et al. 2024, MNRAS,
  535, 2523
Sampson, M., Melchior, P., Ward, C., & Birmingham, S. 2024, A&C, 49,
  100875
Sánchez-Sáez, P., Hernández-García, L., Bernal, S., et al. 2024, A&A,
  688, A157
Sarmah, P., Chakraborty, S., Tamborra, I., & Auchettl, K. 2022, JCAP,
  08, 011
Saulder, C., Howlett, C., Douglass, K. A., et al. 2023, MNRAS, 525, 1106
Schipani, P., Campana, S., Claudi, R., et al. 2018, Proc. SPIE, 10702, 107020F
Schulze, S., Gal-Yam, A., Dessart, L., et al. 2025, Natur, 644, 634
Schulze, S., Krühler, T., Leloudas, G., et al. 2018, MNRAS, 473, 1258
Schutz, B. F. 1986, Natur, 323, 310
Scolnic, D., Kessler, R., Brout, D., et al. 2018, ApJL, 852, L3
Sell, P. H., Maccarone, T. J., Kotak, R., Knigge, C., & Sand, D. J. 2015,
          S, 450, 4198
Senno, N., Murase, K., & Mészáros, P. 2016, PhRvD, 93, 083003
Serrano-Hernández, D. B., Martínez-González, S., Jiménez, S., Silich, S., &
  Wünsch, R. 2025, A&A, 695, A271
Sesar, B., Ivezić, Ž., Lupton, R. H., et al. 2007, AJ, 134, 2236
Shah, V. G., Narayan, G., Perkins, H. M. L., et al. 2024, MNRAS, 528,
Shappee, B. J., Holoien, T. W. S., Drout, M. R., et al. 2019, ApJ, 870, 13
Shappee, B. J., Prieto, J. L., Grupe, D., et al. 2014, ApJ, 788, 48
Sharma, Y., Sollerman, J., Kulkarni, S. R., et al. 2024, ApJ, 966, 199
Shen, K. J., Kasen, D., Miles, B. J., & Townsley, D. M. 2018, ApJ, 854, 52
Shen, K. J., Quataert, E., & Pakmor, R. 2019, ApJ, 887, 180
Shvartzvald, Y., Waxman, E., Gal-Yam, A., et al. 2024, ApJ, 964, 74
Sjoberg, K., Esteves, J., & Stubbs, C. 2025, arXiv:2509.03843
Smartt, S. J., Chen, T.-W., Jerkstrand, A., et al. 2017, Natur, 551, 75
Smirnov, J., Goobar, A., Linden, T., & Mörtsell, E. 2024, PhRvL, 132, 151401
Smith, G. P., Robertson, A., Mahler, G., et al. 2023, MNRAS, 520, 702
Smith, K. W., Williams, R. D., Young, D. R., et al. 2019, RNAAS, 3, 26
Smith, M., Sullivan, M., D'Andrea, C. B., et al. 2016, ApJL, 818, L8
Smith, N. 2014, ARA&A, 52, 487
Smith, N., Ganeshalingam, M., Chornock, R., et al. 2009, ApJL, 697, L49
Snavely, C., Alvarez, G., Hendrix, V., & Cholia, S. 2018, doi:10.6084/m9.
   figshare.7071770.v2
Soares-Santos, M., Holz, D. E., Annis, J., et al. 2017, ApJL, 848, L16
Soderberg, A. M., Gal-Yam, A., & Kulkarni, S. R. 2004, GCN, 2586, 1
Sollerman, J., Fransson, C., Barbarino, C., et al. 2020, A&A, 643, A79 Sollerman, J., Taddia, F., Arcavi, I., et al. 2019, A&A, 621, A30
Souverin, T., Neveu, J., Betoule, M., et al. 2025, RAS Techniques and
  Instruments, 4, rzaf010
Srivastav, S., Moore, T., Nicholl, M., et al. 2023, ApJL, 956, L34
Steeghs, D., Galloway, D. K., Ackley, K., et al. 2022, MNRAS, 511, 2405
Stein, G., Seljak, U., Böhm, V., et al. 2022, ApJ, 935, 5
Stein, R., van Velzen, S., Kowalski, M., et al. 2021, NatAs, 5, 510
Stone, N. C., & Metzger, B. D. 2016, MNRAS, 455, 859
Stone, N. C., & van Velzen, S. 2016, ApJL, 825, L14
Stone, N. C., Vasiliev, E., Kesden, M., et al. 2020, SSRv, 216, 35
Strotjohann, N. L., Ofek, E. O., Gal-Yam, A., et al. 2021, ApJ, 907, 99
Stubbs, C. W., & Brown, Y. J. 2015, MPLA, 30, 1530030
Stubbs, C. W., & Tonry, J. L. 2006, ApJ, 646, 1436
Subrayan, B. M., Milisavljevic, D., Chornock, R., et al. 2023, ApJL, 948,
  L19
Sullivan, M., Conley, A., Howell, D. A., et al. 2010, MNRAS, 406, 782
Sumi, T., Abe, F., Bond, I. A., et al. 2003, ApJ, 591, 204
Taddia, F., Sollerman, J., Leloudas, G., et al. 2015, A&A, 574, A60
```

```
Tanvir, N. R., Levan, A. J., González-Fernández, C., et al. 2017, ApJL,
Tauris, T. M., Langer, N., Moriya, T. J., et al. 2013, ApJL, 778, L23
Tauris, T. M., Langer, N., & Podsiadlowski, P. 2015, MNRAS, 451, 2123
Taylor, E. N., Cluver, M., Bell, E., et al. 2023, Msngr, 190, 46
Terreran, G., Jacobson-Galán, W. V., Groh, J. H., et al. 2022, ApJ, 926, 20
The pandas development team 2020, pandas-dev/pandas: Pandas, latest
   v2.3.2, Zenodo, doi:10.5281/zenodo.3509134
The Rubin Observatory Survey Cadence Optimization Committee 2025,
   Survey Cadence Optimization Committee's Phase 3 Recommendations,
   Vera C. Rubin Observatory, https://pstn-056.lsst.io/
Tonry, J. L., Denneau, L., Heinze, A. N., et al. 2018, PASP, 130, 064505
Toonen, S., Perets, H. B., Igoshev, A. P., Michaely, E., & Zenati, Y. 2018,
    &A, 619, A53
Trakhtenbrot, B., Arcavi, I., MacLeod, C. L., et al. 2019a, ApJ, 883, 94
Trakhtenbrot, B., Arcavi, I., Ricci, C., et al. 2019b, NatAs, 3, 242
Tripp, R. 1998, A&A, 331, 815
Tsalapatas, K., Sollerman, J., Chiba, R., et al. 2025, arXiv:2507.08532
Tsuna, D., & Lu, W. 2025, ApJ, 986, 84
Tucker, M. A., Ashall, C., Shappee, B. J., et al. 2021, ApJ, 914, 50
Tylenda, R., Hajduk, M., Kamiński, T., et al. 2011, A&A, 528, A114
Udalski, A., Szymanski, M., Kaluzny, J., Kubiak, M., & Mateo, M. 1992,
   AcA, 42, 253
Valenti, S., David, S. J., Yang, S., et al. 2017, ApJL, 848, L24
van Roestel, J., Kupfer, T., Green, M. J., et al. 2022, MNRAS, 512, 5440
van Velzen, S., Gezari, S., Hammerstein, E., et al. 2021, ApJ, 908, 4
van Velzen, S., Stone, N. C., Metzger, B. D., et al. 2019, ApJ, 878, 82
Verde, L., Treu, T., & Riess, A. G. 2019, NatAs, 3, 891
Veres, P. M., Franckowiak, A., van Velzen, S., et al. 2024, arXiv:2408.17419
Veres, P. M., Gabányi, K. É., Frey, S., et al. 2021, ApJ, 922, 99
Villar, V. A., Guillochon, J., Berger, E., et al. 2017, ApJL, 851, L21
Villar, V. A., Nicholl, M., & Berger, E. 2018, ApJ, 869, 166
Vivas, A. K., Zinn, R., Andrews, P., et al. 2001, ApJL, 554, L33
```

```
von Kienlin, A., Veres, P., Roberts, O. J., et al. 2019, ApJ, 876, 89
Waldman, R., Sauer, D., Livne, E., et al. 2011, ApJ, 738, 21
Wang, K., Huang, T.-Q., & Li, Z. 2019, ApJ, 872, 157
Ward, C., Melchior, P., Sampson, M. L., et al. 2025, A&C, 51, 100930
Waxman, E., Wasserman, T., Ofek, E. O., & Gal-Yam, A. 2025, ApJ, 978, 133
Wegg, C., Gerhard, O., & Portail, M. 2017, ApJL, 843, L5
Wevers, T., Pasham, D. R., van Velzen, S., et al. 2021, ApJ, 912, 151
Wiseman, P., Wang, Y., Hönig, S., et al. 2023, MNRAS, 522, 3992
Wiseman, P., Williams, R. D., Arcavi, I., et al. 2025, MNRAS, 537, 2024
Woosley, S. E., Blinnikov, S., & Heger, A. 2007, Natur, 450, 390
Woosley, S. E., Eastman, R. G., Weaver, T. A., & Pinto, P. A. 1994, ApJ,
  429, 300
Wyrzykowski, Ł., Kostrzewa-Rutkowska, Z., Skowron, J., et al. 2016,
    INRAS, 458, 3012
Yan, L., Lunnan, R., Perley, D. A., et al. 2017a, ApJ, 848, 6
Yan, L., Quimby, R., Gal-Yam, A., et al. 2017b, ApJ, 840, 57
Yao, Y., Chornock, R., Ward, C., et al. 2025, ApJ, 985, L48
Yao, Y., Guolo, M., Tombesi, F., et al. 2024a, ApJ, 976, 34
Yao, Y., Lu, W., Guolo, M., et al. 2022, ApJ, 937, 8
Yao, Y., Lu, W., Harrison, F., et al. 2024b, ApJ, 965, 39
Yao, Y., Ravi, V., Gezari, S., et al. 2023, ApJL, 955, L6
Yaron, O., Perley, D. A., Gal-Yam, A., et al. 2017, NatPh, 13, 510
Yoachim, P. 2025, lsst-sims/sims_featureScheduler_runs4.3: Initial Release,
  v1.0, Zenodo, doi:10.5281/zenodo.14920193
Yuan, F., Kobayashi, C., Schmidt, B. P., et al. 2013, MNRAS, 432, 1680
Yuan, W., Zhang, C., Ling, Z., et al. 2018, Proc. SPIE, 10699, 1069925
Zackay, B., Ofek, E. O., & Gal-Yam, A. 2016, ApJ, 830, 27
Zenati, Y., Perets, H. B., Dessart, L., et al. 2023, ApJ, 944, 22
Zenati, Y., Perets, H. B., & Toonen, S. 2019, MNRAS, 486, 1805
Zhai, R., Rodriguez, A. C., Mao, S., et al. 2025, ApJ, 978, 76
Zhang, K., Wang, X., Zhang, J., et al. 2016, ApJ, 820, 67
Zimmerman, E. A., Irani, I., Chen, P., et al. 2024, Natur, 627, 759
Zirakashvili, V. N., & Ptuskin, V. S. 2016, APh, 78, 28
```